Aus dem Institut für Pathologie

der Medizinischen Fakultät Mannheim

(Direktor: Prof. Dr. med. Alexander Marx)

IGF1R and TYRO3 as potential biomarkers for response prediction in malignant thymomas and thymic carcinomas treated with sunitinib

Inauguraldissertation

zur Erlangung des Doctor scientiarum humanarum (Dr. sc. hum.)

der

Medizinischen Fakultät Mannheim

der Ruprecht-Karls-Universität

zu

Heidelberg

vorgelegt von

Stefan Thomas Küffer

aus

Thun, Schweiz

1974

Diese Arbeit widme ich meinem Vater.

Das Leben ist durchaus nicht so konsequent wie unsere

Sorgen, es hat viel mehr Einfälle und viel mehr Seiten als wir.

Rainer Maria Rilke (1875 - 1926)

Dekan: Prof. Dr. med. Sergij Goerdt

Referent: Prof. Dr. med. Alexander Marx

CONTENT

ABBREVIATIONS

AChR	Acetylcholine receptor
AIRE	Autoimmune regulator
APC	Antigen-presenting cell
BSA	Bovine serum albumin
c-KIT	Tyrosine-protein kinase kit or CD117
CSF1	Colony-stimulating factor 1
DAPI	4',6-Diamidino-2-phenylindole dihydrochloride
DC	Dendritic cell
DMEM	Dulbecco's Modified Eagle's Medium
DMSO	Dimethylsulfoxide
DNA	Deoxyribonucleic acid
dNTP	Desoxyribonucleosidtriphosphate
EDTA	Ethylenediaminetetraacetic acid
EGFR	Epithelial growth factor receptor
EMT	Epithelial-mesenchymal transition
ERK	Extracellular signal-regulated kinase
FACS	Fluorescence-activated cell sorting
FDA	U. S. Food and Drug Administration
FLT3	FMS-like tyrosine kinase 3
FOXN1	Fork head factor N1
GAPDH	Glyceraldehyde 3-phosphate dehydrogenase
GAD56	Glutamate decarboxylase 56
GIST	Gastrointestinal stroma tumor
H2Ax	H2A histone family member X
HRAS	Transforming protein p21
HRP	Horseradish peroxidase
Hsp27	Heat shock protein 27
IGF-1R	Insulin-like growth factor 1 receptor
IHC	Immunohistochemistry
IR	Insulin receptor
LRP4	Lipoprotein receptor-related protein
MAPK	Mitogen-activated protein kinase

Abbreviations

MHC	Major histocompatibility complex
MSP R	
mTEC	Medullar thymic epithelial cell
MTS	3-(4,5-Dimethylthiazol-2-yl)-2,5-diphenyltetrazolium bromide
MuSK	Muscle tyrosine kinase
OS	Overall survival
p53	Tumor protein p53
PBS	Phosphate-buffered saline
PCR	Polymerase chain reaction
PDGFα	Platelet-derived growth factor α
PDGF R β	Platelet-derived growth factor receptor β
PFS	Progression-free survival
PI3K/Akt	Phosphoinositid-3-kinase/ protein kinase B
qRT-PCR	Quantitative reverse transcription PCR
RCC	Renal cell carcinoma
RIPA	Radioimmunoprecipitation assay buffer
RNA	Ribonucleic acid
RPM	Rounds per minute
RPMI	Roswell Park Memorial Institute
RET	RET proto-oncogene
SRI	Sunitinib response index
siRNA	Small interfering RNA
TC	Thymic carcinoma
TH	Thymoma
TKI	Tyrosine kinase inhibitor
TSCC	Thymic squamous cell carcinoma
TP53	Tumor protein P53
TYRO3	Tyrosine-protein kinase receptor

1   INTRODUCTION

1.1   The Thymus

1.1.1 Development and structure

The thymus (from the Greek word θυμός, thymos) is a primary lymphoid organ responsible for the maturation of T cells. The thymus develops from the ventral endoderm of the third pharyngeal pouch and is located in the anterior mediastinum, in front of the heart and behind the sternum. The mature thymus shows a lobular structure, and each lobe is made up of a central medulla and a peripheral cortex. Under the influence of forkhead factor N1 (FOXN1), cortical and medullar epithelial cells develop from an endodermal precursor cell. Cortical epithelial cells are characterized by the expression of CD205, „major histocompatibility complex" class II (MHCII), thymus proteasome and different cathepsins (e.g. cathepsin L). Medullar epithelial cells are CD205-negative and express e.g. CD40 und claudin 4[1, 2]. Epithelial cells in the medulla are more densely packed than in the cortex. In addition, there are hypercellular squamous epithelial structures called Hassall's corpuscles that most likely represent terminally differentiated medullar epithelial cells[3] (Figure 1).
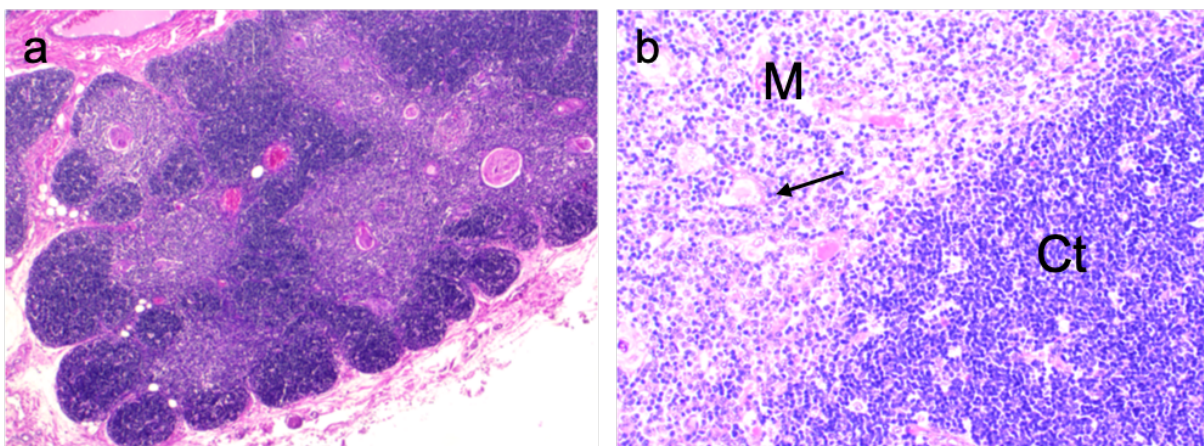

Figure 1: Low power view shows the lobular architecture of the thymus of a young child (a). The darker cortex (Ct) is dominated by small lymphocytes, while in the lighter medulla (M), epithelial cells predominate. Numerous Hassall's corpuscles of different sizes are located in the medulla (arrow) (b).

Introduction

1.1.2 Function and involution

As a primary lymphatic organ in all higher vertebrates, the thymus plays a critical role in the establishment of a functional repertoire of mature T cells, and is therefore a central component of the adaptive immune system. The most important function of the thymus is the establishment of a T cell repertoire that effectively protects against infection but also tolerates self-antigens. In addition to thymic epithelial cells, dendritic cells (DC) and macrophages belong to the so-called professional antigen-presenting cells (APC) and are distinguished by constitutive expression of the MHCII and the ability to present bound antigens to T cells. The two most important steps during T cell development are the so-called positive and negative selection. During positive selection, T cells recognize MHC on APCs and survive. T cells that do not recognize MHC antigens will die of neglect. Positive selection takes place in the thymic cortex. Negative selection occurs mainly in the thymic medulla and is a process in which T cells that bind the MHC-antigen complex with too high affinity are eliminated as potentially autoreactive. Both cortical and medullary epithelial cells represent heterogeneous cell populations with different functions. The ectopic or promiscuous expression of tissue-specific self-antigens is a central function of medullary thymic epithelial cells (mTECs). A subgroup (5-10%) of mTECS positive for the autoimmune regulator AIRE express about 3,000 genes from brain, liver, kidney, pancreas and other organs. About 98-99% of all immature thymocytes are eliminated in the thymus, and only about 1% with a medium receptor affinity receive a survival signal, leave the thymus and move to the periphery[4, 5].

Thymic involution begins already between the ages of 5-10 and is completed between the 5th and the 6th decades[6]. At this time, the thymus consists of about 95% fatty tissue. However, the residual 5% thymus remains active until old age. Thymic involution is presumably determined by genetic and hormonal factors[7]. The switching off of the homeodomain transcription factor Meis1, which is highly expressed in immature mTECs and contributes to the maintenance of a progenitor phenotype and the down-regulation of FOXN1, seem to be essential. Castration delays or even inhibits involution in animal models. The interaction with thymocytes also seems to be crucial for the conservation of the thymus, since experimental T cell depletion results in thymic involution[7]. With increasing age, thymic involution leads to a decreased export of mature naive T cells from the thymus to the periphery. Starting with the 4th decade of life, the thymus is no longer able to fulfil the need for new T cells, and its T cell

repertoire dwindles. This leads to the replacement of old peripheral T cells through homeostatic proliferation instead of new T cells from the thymus. Among other changes, senescent T cells downregulate CD28 and become resistant against apoptosis. T cells thereby begin to express genes that are normally expressed in natural killer cells which belong to the innate immune system. In addition, senescent cells have the tendency to produce increasing amounts of pro-inflammatory cytokines and reduce the response to regulatory signals. This increases the risk of inflammatory tissue damage[5]

1.2   Myasthenia gravis

Myasthenia gravis (MG) is an autoimmune disease that develops through the production of different autoantibodies against proteins of the neuromuscular end plate. The symptoms of MG consist of a fluctuating muscle weakness with remission and exacerbation, which can first manifest itself as ocular MG in the form of double images and ptosis. The most important antigen targets against which autoantibodies are directed are the acetylcholine receptor (AChR; about 80% of all cases), the muscle tyrosine kinase (MuSK; about 10%) and the lipoprotein receptor-related protein (LRP4; about 5%). Autoimmune antibodies against AChR are found in three different clinical settings: in patients before the 5th decade with so called early-onset MG, in patients over 60 with so-called late-onset MG, and in patients of any age with thymoma (so-called paraneoplastic MG. The etiology of autoimmune reactions against AChR is not known, but certain genetic factors such as HLA-B8 DRB1*03, DQA1*0501 and DQB1*0201 as well as risk alleles of PTPN22 und TNIP1 may contribute to hyperinflammatory reactions of the thymus[8, 9].

1.3   Thymic malignancies

About 25% of all mediastinal tumors are malignant. 65% are epithelial tumors, divided into thymomas (TH) and thymic carcinomas (TC) (50% of cases), followed by lymphomas (25%), neuroendocrine tumors (15%), and germ cell tumors (10-15%)[10, 11]. TH are subclassified into the more indolent types A, AB and B1, and the more aggressive types B2 and B3. TC are further subclassified into squamous cell, basaloid,

lymphoepithelioma-like, neuroendocrine and many other types. The differentiation between TH and TC is based on morphological, biological and clinical factors. The neoplastic epithelium in TH still contains functions of the normal thymic epithelium and interacts with immature T cells. Therefore, the immunohistochemical identification of immature T cells is an important clue to the diagnosis of a TH. All TH types have malignant potential and can recur locally and ¹²⁸ₒₐᵢ. Currently, two alternative staging systems are in use: the older Masaoka-Koga system and the more recent UICC TNM classification (Table 1).

1.3.1 Thymoma

1.3.1.1 Type A thymomas

At about 12% of all thymomas, Type A TH represents the smallest group. The median age is 64 (8-88) and males seem to be a bit more frequently affected than females[13]. Histologically, there are different growth patterns (fascicular, storiform, adenoid and glomeruloid)[14], and they can occur next to each other in one tumor. Hassall bodies are not found, and there are no or only few immature T cells. Cases with >10% of the tumor area containing a moderate or high content of TdT-positive immature T cells are classified as Type AB TH. The epithelial component of Type A TH is strongly positive for CK19 and p63 and negative for CK20, CD5 and CD117. Complete resection is the therapy of choice and is usually feasible. The 10-year survival rate ranges between 80-100%. Metastases are observed, but are very rare[12, 15].

1.3.1.2 Type AB thymomas

Type AB thymomas contain a lymphocyte-poor (type A) and a lymphocyte-rich (type B) component in varying proportions. In 20-40% of cases, type AB is the most common TH subtype. The median age is 57 (11-89). Genetic alterations are more frequent in type AB than in type A TH, but there may be a relationship between the two. In type AB (and A thymomas), *GTF2I* mutations are frequent (74%). 20-40% of the cases are associated with myasthenia gravis and almost 95% of the tumors are in Masaoka-Koga

Introduction

Table 1: Staging after Masaoka-Koga and after UICC TNM (8th edition, 2017) [16].

Stage	Masaoka-Koga	ITMIG	
I	Grossly and microscopically encapsulated. Also called a non-invasive thymoma because it has not spread beyond the thymus.	T1a:	Encapsulated or unencapsulated, with or without extension into mediastinal fat
II	The thymoma extends beyond the capsule (outer boundary of the thymus) and into the nearby fatty tissue or to the pleura (outer covering of the lung). Sometimes divided into:	T1b:	Extension into mediastinal pleura
IIa	Microscopic transcapsular invasion	T2:	Infiltration of the pericardium
IIb	Macroscopic capsular invasion	T3:	Infiltration of one of the following structures: Lung, brachiocephalic vein, superior vena cava, chest wall, phrenic nerve, hilar (extrapericardial) pulmonary vessels
III	Macroscopic invasion of neighboring organs. The thymoma extends into the neighboring tissues or organs of the lower neck or upper chest area, including the pericardium (covering of the heart), the lungs, or the main blood vessels leading into or exiting from the heart.	T4:	Infiltration of one of the following structures: Aorta, arch vessels, main pulmonary artery, myocardium, trachea, or esophagus
IVA	Pleural or pericardial dissemination. The thymoma has spread widely throughout the pleura and/or pericardium.		
IVB	Hematogenous or lymphatic dissemination. The thymoma has spread to distant organs		

stage I or II at diagnosis. Higher tumor stages are associated with atypical histological features, e.g. necrosis. The epithelial component expresses keratins and p63, and in 20-30% CD20. The ki67 index is usually <10%. The lymphocytic component contains mainly CD3- and TdT-positive immature T cells with a high ki67 index. Complete surgical resection is the treatment of choice. The 10-year survival rate ranges between 80 and 100% with very few documented metastases[14].

1.3.1.3 Type B1 thymomas

Type B1 thymomas closely resemble normal thymus with extensive cortical and medullary areas with or without Hassall bodies. They represent about 18% of all cases and occur slightly more frequently in women. The median age is 57 years of age (6-83). Coughing, thoracic pain and dyspnea are typical symptoms in two-thirds of the patients. 35-45% of the cases are associated with myasthenia gravis. Almost 90% are in Masaoka-Koga tumor stage I or II at the time of diagnosis. Infiltration of neighboring organs and metastases are very rare events. Over 90% of all type B1 TH are locally resectable, and a recurrence is rare, resulting in a 10 to 20-year survival rate in 85-100% of patients[14].

1.3.1.4 Type B2

Type B2 thymomas are lymphocyte-rich epithelial tumors with a high risk of intrathoracic recurrence. They make up about 25-30% of all cases and are evenly distributed between females and males. The median age is 50 years with only single cases described in adolescents and children. In contrast to normal thymus or type B1 TH, cortical differentiation is slightly reduced in type B2 TH, and medullary differentiation is clearly less developed. About half of the cases are accompanied by myasthenia gravis. About 30% are diagnosed as stage III and 10% as stage IV. Distant metastases (Masaoka-Koga stage IVb) are observed in about 3%. Type B2 TH express numerous keratins (e.g. AE1/3, CK19) and p63. The superimposed lymphocytes are mainly immature, CD3/TdT-positive immature T cells. Complete surgical resection is the therapy of choice and can be achieved in about 70-90% of cases. The recurrence rate of totally resected tumors in Masaoka-Koga stage II after 10 years is about 32%, and 41% for tumors in stage III. Therefore, postoperative radiotherapy is recommended for all stage III tumors. Multimodal concepts with preoperative chemotherapy followed by resection and postoperative radio-chemotherapy of primary non-resectable tumors are recommended. The overall 10-year survival rate is between 70-90%[14, 17].

1.3.1.5 Type B3 thymomas

Type B3 thymomas are predominantly epithelial thymic tumors with rare but mostly immature T cells. The neoplastic epithelial cells show an extensive loss of the cortical and an almost complete loss of the medullary differentiation. They comprise up about 15-20% of all cases and men are a slightly more frequently affected than women. The median age is 55 years (8-87). Most patients come to clinical attention through local symptoms such as thoracic pain or vena cava superior syndrome. 40-50% of the cases are associated with myasthenia gravis[13]. 50% of the tumors are diagnosed as Masaoka-Koga stages I and II, about 30% as stage III, and about 20% as stage IV. Type B3 TH often show infiltration of neighboring structures such as great vessels, pericardium, or lung. The tumor epithelium expresses various cytokeratins such as CK19, CK5/6, CK8/18 und p63 plus focally EMA. In contrast to Type A and AB TH, CD20 is not expressed, and CD5 and CD117 are also usually negative. The sparse lymphocytes are predominantly immature TdT-positive T-cells. The therapeutic concepts are the same as for Type B2 TH. Up to 30% of the cases show a recurrence after some years and the 10-year survival rate is 50-70%[5].

1.3.2 Thymic carcinoma (TC)

Like TH, TC are also tumors of the thymic epithelium. In contrast to TH, the neoplastic epithelium in TC has usually lost its organotypic properties and is not able to mature T cells. This is believed to be the reason why TC are not associated with myasthenia gravis. The discrimination between TC and TH is of great clinical relevance. In most published cohorts, TC had a much worse prognosis than thymomas. In contrast to thymomas, which virtually never show lymph node metastases, regional lymph node metastases are observed in about 30% of TC[18]. TC also have a high risk of distant metastases (about 50%), whereas thymomas tend to be limited to the thoracic cavity and only metastasize outside the thorax in about 15%. The incidence of TC is 1 in 10 million inhabitants per year and elderly males and females are equally affected. TC are further subclassified into squamous cell, basaloid, lymphoepithelioma-like, neuroendocrine and many other subtypes. The therapy of TC is in principle the same as for thymomas, but it has been shown that postoperative radiotherapy of R0-resected stage II tumors results in improved progression-free (PFS) and overall survival (OS)[19]. R1-resected TC should be treated with postoperative radio-chemotherapy. Apart from

the resection status, the Masaoka-Koga stage is also considered a prognostically relevant factor with a 10-year survival of 60% in stage I vs. 15% in stage IV[20].

1.3.3 Molecular pathology of TH and TC

The histological classification of the WHO of TH and TC has been shown to correlate with clinical risk factors such as tumor stage, clinical behavior, and prognosis, suggesting an increasing mutational load from type A to TC [21]. However, even though multi-omics platform analyses of 117 TET demonstrated a marked prevalence of a thymoma-specific mutated oncogene, *GTF2I*, in type A and AB TH, TH and TC were among the tumors with the lowest mutational burden of all adult cancers. Rare tumor-relevant mutations such as *HRAS*, *NRAS*, *TP53*, even when present, are not targetable[22]. A previous study described an almost mutually exclusive loss of 13q in B3 and TC at a frequency of 15% which was associated with disease progression, and another group found a rare but also clinically relevant loss of 9p21.3 encoding p16INK4 and p14ARF in B3 and TC[23, 24]. Gain of 1q containing the anti-apoptotic MCL1 gene was observed in 51% of all subtypes, with a higher frequency in B3 (70%) and TC (57%). A copy number gain in the *BCL2* locus (18q21.33) with a frequency of up to 42% in TC is also present in type A and B3 TH. The overexpression of Bcl-2 correlates with decreased survival in TET, which is why targeting Bcl-2 has been suggested as a combinatorial treatment[25]. TC also seem to be enriched for mutations in epigenetic regulatory genes, among them *TP53* which is found in 30-40% of the cases. The mutation correlates with an increased IHC staining and is of prognostic relevance[26, 27]. Rare cases had an activating mutation of the *KIT* gene with a good response to imatinib[28].

1.3.4 Treatment and response prediction of advanced thymoma and TC

Complete resection is the basis for the successful treatment of mediastinal tumors. However, in advanced TET, where complete removal is not always possible, patients seem to also profit from the decreased tumor load. For Masaoka-Koga stages I and II, an expanded thymomectomy (R0 resection) including fat tissue is recommended. According to ESMO (European Society for Medical Oncology) and NCCN (Clinical

Introduction

Practice Guidelines in Oncology) guidelines, radiotherapy should be taken into consideration for cases of Masaoka stage II. The primary therapy goal for the Masaoka-Koga-stages III und IVa/IVb is complete resection. In non-resectable but functionally operable TH and TC patients, cisplatin-based regimens such as the PAC scheme (cisplatin, adriamycin, cyclophosphamid) or alternative cisplatin-/ etoposid-based therapies are most often used[29]. Relapses or progressive disease can be expected to occur in 10 – 30 % of all patients. In 20-30% of these patients, objective remissions can be achieved by cisplatin-based regimens after relapse-free intervals of 6-12 months[30]. Approximately 50 % of patients with an advanced malignant TH or TC are candidates for a second-line treatment. Aberrant EGFR, c-KIT and IGF-1R signaling and angiogenesis as well as mTOR inhibition have been shown to be targetable molecular biomarkers involved in the carcinogenesis, growth and different behaviors of thymic tumors. However, whereas sunitinib, somatostatin receptor inhibitors, everolimus and anti-IGF1R have shown some specific activity, other agents have shown little to no clinical advantages [28] [30-34]. The variable clinical results suggest that a broader approach is necessary to obtain satisfactory therapeutic results in a relevant proportion of patients with malignant TETs.

1.4 Sunitinib as a second-line therapy option in TH and TC

In recent years, multi-tyrosine-kinase inhibitors (TKIs) have been successfully used for a broad range of malignant tumors, including renal and liver cancer and melanoma. Sunitinib (Sutent, Pfizer) belongs to one of the multi-target TKI that has been approved by the FDA for treatment of renal cell carcinomas (RCC)[35] and imatinib-resistant gastrointestinal stromal tumors (GIST). Sunitinib is a very broad inhibitor that impairs cellular signaling by targeting multiple RTKs, including all receptors for platelet-derived growth factor (PDGF-Rs) and vascular endothelial growth factor receptors (VEGFRs) [36]. However, it is also known to block the intracellular ATP-binding sites of several other RTKs such as VEGF1, VEGF3, FLT3, c-KIT, PDGFα, CSF1, and RET [37].

Sunitinib also seems to be a good option for second-line therapy in patients with metastatic TC[38]. In an open-label phase 2 trial it was demonstrated that sunitinib was active in 26% of the patients with pretreated TC, whereas activity was limited to only 6% in patients with thymoma (Type B3). Molecular profiling of receptor tyrosine kinases known to be sunitinib targets, including PDGFRA, FLT3, and KIT showed somatic

variations in 62% of TC, but they were not predictive of response to sunitinib[39]. In a different study, three patients with histologically and immunohistochemically comparable TCs that showed no mutations in c-KIT, KRAS, BRAF, or EGFR were treated with sunitinib. Screening for activated RTK revealed a heterogenous activation of EGFR, EphB2, KIT, IR, RON, Erb4, FGFR2, KIT, IGF1R, RET and Tyro3/Dtk with the strongest activation in EGFR, TYRO3/DTK and IGF1R. TC seem to be responsive to sunitinib, and the therapy is certainly of some benefit. However, due to the acquired resistance and potential toxicities of sunitinib, there is need for more refined approaches based on biomarkers and patient selection that will help identify the most efficacious treatment[39, 40]. It is also important to investigate whether patients with malignant TH may also benefit from this drug.

1.5 A tyrosine kinase peptide array to predict TKI response

Aberrant RTK signaling activity occurs in tumors that are more resistant to TKI treatment. In consequence, RTK activity arrays should be able to distinguish between signatures[41]. Kinase activity profiling could also be a valuable clinical tool to select TKI treatment for patients with advanced cancer, enhancing the efficacy of available drugs and facilitating the choice of possible new approaches. The PamChip microarray contains 144 tyrosine kinase peptide substrates representing key signal transduction pathways (PamGene, Den Bosch, The Netherlands). This technology directly measures the mechanism of action of a kinase inhibitor by building the ratio of kinase activity in the lysate in the absence of a compound over the activity in the presence of a compound. Whether the kinase activity measurement or the application of a phospho tyrosine kinase (PTK) microarray for the identification of responders versus non-responders is more accurate is still under discussion[42-46]. The PamGene array is a robust screening method that allows measurement and evaluation of tissue lysates from individual patients spiked in with available drugs or drug combinations. Consisting of a porous membrane, the lysate is repeatedly pumped through the array, thus enabling a 'kinetic' measurement of phosphorylation changes over time (**Fig. 2**). Spot intensities on the arrays are derived from an anti-phosphotyrosine antibody that binds to the peptide substrates which become phosphorylated by kinases present in the sample. By inducing a drug resistance in cell lines, this method allows measurement of specific drug resistance phospho-patterns. The resistance pattern can then be used

to generate a specific prediction quantifier. This quantifier can be applied to the phospho-patterns of patient tissue samples and predicts, to a certain degree, the response of the tumors to the specific TKI treatment[42]
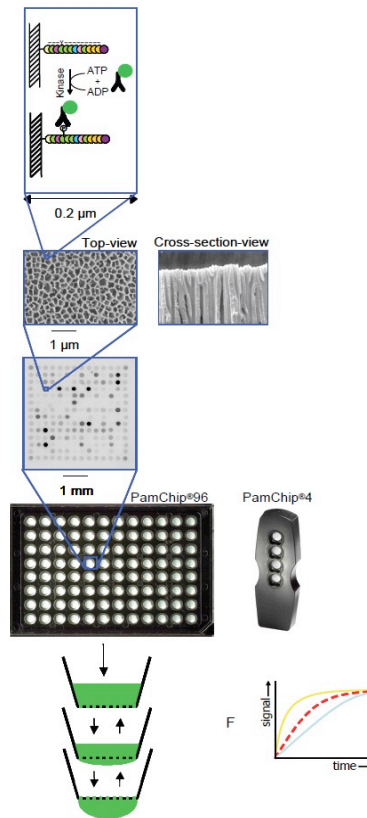
Figure 2: Schematic representation of a PamChip microarray (PamGene). 144 15mer polypeptides containing a tyrosine at the middle position (top) are attached to the surface of a porous three-dimensional chip (middle). Cell lysate-antibody mixture is pumped up and down through the array and increasing phospho antibody signal is measured by a high sensitivity camera (bottom). Modified from pamgene.com.

1.6   Insulin-like growth factor receptor 1 (IGF-1R)

The IGF-1R is a transmembrane receptor tetramer consisting of two extracellular $\alpha-$subdomains and two transmembrane $\beta-$subdomains that are connected through disulfide bonds. The two $\alpha-$subunits form the 130-135 kDa ligand binding site and the 90–95 kDa $\beta-$subdomains contain the tyrosine domains [47]. IGF-1R is activated by

IGF1 and IGF2. The bound ligand leads to an autophosphorylation of the intracellular tyrosine residues of the $\beta-$subdomain. This in turn leads to IGF-1R signaling and to an activation of the PI3K/Akt anti-apoptotic signaling pathway. In addition, IGF-1R activation results in increased cell proliferation over Shc, Ras, Raf − 1/MEK/ERK activation. IGF-1R has been shown to be overexpressed in up to 37% of tumors?? cases?? and is amplified in up to 26% in TC. Deregulation of IGF2 is another main factor behind intensified IGF signaling [48].

1.7 TYRO3/Dtk

TYRO3/Dtk belongs to the TAM (TYRO3/Dtk , Axl, MerTK) family of RTKs. Each member contains an extracellular domain consisting of two immunoglobulin-like domains and two fibronectin type III repeats, a transmembrane portion, and a cytoplasmic domain with the tyrosine kinase. The human TYRO3/Dtk is located on chromosome 15 and the protein contains 890 amino acids with a predicted molecular weight of 97 kDa. Due to post-translational modifications, the actual molecular weight ranges between 120-140 kDa[49, 50]. TYRO3/Dtk has a restricted tissue expression profile and has been implicated in various biological functions, including myelination in the brain[51]. Current data suggest that, like other TAM kinases, TYRO3/DTK functions in tumor cells to activate common oncogenic signaling pathways, particularly MEK/ERK and PI3K/AKT. However, other downstream pathways are likely to play critical roles in tumorigenesis as well. Regulation of cell type-specific effectors downstream of TYRO3/DTK has also been reported in specific tumor types, including microphthalmia-associated transcription factor (MITF) in melanoma and alpha-fetoprotein (AFP) in hepatocellular carcinoma[50, 52-54]. Overexpression of TAMs and their major ligand growth arrest-specific factor 6 (Gas6) is associated with more aggressive behavior of cancers, poorer patient survival, acquired drug resistance and metastasis. A role of TYRO3/DTK in cancer has been discussed since its discovery, particularly due to its proven function in cell proliferation and survival in several cancer cells as well as its correlation to ligand overexpression with poor prognosis of several tumor types, including thyroid cancer. In addition, TYRO3/Dtk has also been implicated in the resistance to traditional chemotherapies and molecularly targeted agents[50].

1.8 Hypothesis

The FDA-approved TKI sunitinib is regarded as feasible for second-line therapy in patients with progressive TH and TC. Even though sunitinib activity in TC is high in comparison with other second-line treatments, it has no beneficial effect in the majority of TC as well as in almost all malignant TH cases. The acquired resistance and potential toxicities connected to this drug underline the need to identify other approaches based on biomarkers and patient selection to develop the most effective individual treatment protocols [39, 40]. Kinase activity profiling has also been proposed as a valuable clinical tool for selecting patients with advanced cancers to undergo TKI treatment. This would enhance the efficacy of available drugs for a more personalized medicine and a more accurate response prediction.

1.9 Aim of the study

The present study aimed to predict response to sunitinib in patients with advanced TC and TH. To this end, we combined phospho RTK and MAPK arrays and a multiplex tyrosine phosphorylation assay (PamGene) to detect potential biomarkers. One of the goals was to generate a sunitinib response index (SRI) using sunitinib-resistant cell lines that can be applied to patient samples. The application of the SRI, the prediction of the upstream kinases and the combined analysis with the specific RTK and MAPK activity provides important information on the response to sunitinib as well as potential new sunitinib targets in malignant TH and TC.

2 MATERIAL AND METHODS

2.1 Chemicals and kits

2.1.1 Chemicals and reagents

Tab. 1 Chemicals and reagents

Product	Company
Annexin V Binding Buffer **APC Annexin V**	BioLegend, California, USA
Laemmli Sample Buffer 4x **TGS 10x Running Buffer**	BioRad, München, Germany
Ampicillin sodium salt **LB medium** **Milk powder** **Ponceau S** **Tris Pufferan**® **Tris hydrochloride (Tris-HCl) Pufferan**® **Sodium chloride (NaCl)**	Carl Roth GmbH, Karlsruhe, Germany
Ethanol (100%) (EtOH) **Isopropyl** **Paraformaldehyde**	Chemsolute®, Renningen, Germany
Fetal calf serum (FCS) **L-Glutamine** **Penicillin / Streptomycin** **RPMI-1640** **Trypsin**	Gibco, Darmstadt, Germany
Dimethylsulfoxide (DMSO)	Honeywell, Bucharest, Romania

PBS Dulbecco 10x	Merck, Darmstadt, Germany
Re-Blot Plus Strong Solution 10x	
Puregene® Proteinase K	Qiagen GmbH, Hilden, Germany
RNase A Solution	
RNase free water	
Xtreme GENE HP DNA Transfection Reagent	Roche, Mannheim, Germany
Tissue-Tek® O.C.T. Compound	Sakura Finetek , Leiden, Netherlands
β-Mercaptoethanol	Sigma-Aldrich, Taufkirchen, Germany
DAPI	
IGEPAL® CA-630	
Sodium deoxycholate	
Sodium orthovanadant	
Sunitinib Malate	
Tween® 20	
Pierce® 660nm Protein Assay Reagent	Thermo Fisher Scientific Inc.,
Pre-Diluted Protein Assay Standards: BSA Set	Massachusetts, USA
Protein Ladder (PageRuler™ Prestained Protein Ladder)	
Triton® X-100 Surface-Amps® Detergent Solution	

2.1.2 Consumables

Tab. 2 Consumables

Product	Company
Mini-PROTEAN® TGX™ Precast Gels	BioRad, München, Germany

Polystrene Round-Bottom Tube (5ml)	Corning®, New York, USA
Combitips advanced **Tubes (1.5ml, 2ml)**	Eppendorf AG, Hamburg, Germany
Whatman filter	GE Healthcare, Freiburg, Germany
Tube (15ml, 50ml)	Greiner Bio-one, Frickenhausen, Germany
PCR tube 8 strip (0.2ml)	STARLAB GmbH, Hamburg, Germany
Cell scraper 25cm **CryoPure (1.8ml)** **Pipet tips** **Serological pipettes (5ml, 10ml, 25ml)**	Sarstedt, Nürnbrecht, Germany

2.1.3 Commercial kits and standards

Tab. 3 Commercial kits and standards

Product	Company
DC^{TM} Protein Assay **Trans-Blot® Turbo^{TM} RTA Transfer Kit, Nitrocellulose**	BioRad, München, Germany
Muse Count & Viability Kit	Merck, Darmstadt, Germany
Plasmid Midi Kit (25) **Puregene® Blood Kit** **QIAxcel® DNA Screening Cartridge**	Qiagen GmbH, Hilden, Germany
Western Lightning® Plus-ECL	Perkin Elmer Inc., Massachusetts, USA

CellTiter 96® AQueous One Solution Cell Proliferation Assay	Promega, Mannheim, Germany
Proteome ProfilerTM Array, Human phospso-RTK Array Kit **Human Phospho-MAPK Array Kit**	R&D Systems Inc., Minnesota, USA

2.1.4 Equipment

Tab. 4 Equipment

Product	Company
Sonoplus HD70	Bandelin electronic GmbH&CoKG, Berlin, Germany
Incubator	Binder, Tuttlingen, Germany
Mini Trans-Blot Cell (WB) **Trans-Blot® TurboTM Transfer System** **PowerPac 200**	BioRad, München, Germany
Pipetboy Accujet 1000	Brand, Wertheim, Germany
Centrifuge 5417R **Centrifuge 5424** **Thermomixer C** **Multipipette plus**	Eppendorf AG, Hamburg, Germany
Muse Cell Analyzer	Merck, Darmstadt, Germany
Microm HM550	Microm International GmbH, Walldorf, Germany

PamStation 12® Workstation Processing Flow-Through PamChip arrays	PamGene, 's-Hertogenbosch, The Netherlands
Fusion FX Western Blot Detection System	Peqlab, Erlangen, Germany
peqSTAR Thermal Cycler	
QIAxcel® Advanced Instrument	Qiagen GmbH, Hilden, Germany
Vortex Genie 2	Scientific Industries Inc., New York, USA
Plate reader infinite M200 Pro	Tecan Group Ltd., Männedorf, Switzerland
NanoDrop ND-1000 Spectrophometer	Thermo Fisher Scientific Inc., Massachusetts, USA

2.1.5 Software

Tab. 8 Software

software	company
ND-1000 V3.8.1	Peqlab
Image J Version 1.52j	National Institutes of Health and the Laboratory, Bethesda, USA
i-control™	Tecan Trading AG, Männedorf, Schweiz
Magellan™	
Fusion	Vilber Lourmat, Collégien, Frankreich
Microsoft Excel	Microsoft Corporation, Redmond, Washington, USA
GraphPad Prism 7	GraphPad Software, La Jolla, Kalifornien, USA

2.1.6 Buffers and solutions

Tab. 7 Buffers and solutions

Buffer/solution	Ingredients
Ponceau S solution	0.1% Ponceau S, 1% Acetic acid (100%) diluted in ddH$_2$O
RIPA buffer	0.5% Sodium deoxycholate, 1% IGEPAL CA-360 (NP-40), diluted in 1x PBS (pH 7.4)
Protein lyses buffer	RIPA buffer, complete x EDTA, 1mM PMSF, 1nM Sodium orthovanadant
10x TBS	292,7g NaCl (5M), 4,24g Tris (0.035M), 0,165g Tris-HCl (0.165M), diluted in 1l ddH$_2$O
TBST	1xTBS, 0.1% Tween® 20, diluted in ddH$_2$O

2.1.7 Biological material

2.1.7.1 Human cell lines

Tab. 9 Human cell lines

Cell line	Type	Company
1889c	Thymic carcinoma	A kind gift[55] of Prof. Ralf J. Rieker, Institute of Pathology, University Hospital, Heidelberg, Germany
Caki1	Kidney cancer	American Type Culture Collection (ATCC), Virgina, USA
Caki2	Kidney cancer	
HCT116	Colorectal cancer	
MCF7	Breast cancer	
PC3	Prostate cancer	
TAB1	Thymoma type AB	Originally published as IU-TAB-1[55] and a kind gift of Prof. Loehrer PJ Sr

		Department of Medicine, Indiana University School of Medicine, USA

2.1.7.2 siRNAs

Tab. 10 siRNAs

Product	Catalog no	Company
Hs_TYRO3_5	SI00288344	Qiagen GmbH, Hilden, Germany
Hs_TYRO3_6	SI00288351	
Hs_IGF1R_11	SI05076827	
Hs_IGF1R_12	SI05076834	
AllStar Negative Control siRNA	SI03650318	

2.1.7.3 Prokaryotic cells

E.Coli strain DH5α (Subcloning Efficiency^{TM} DH5α^{TM}) was purchased from Thermo Fischer Scientific Inc., Massachusetts, USA.

2.1.7.4 DNA plasmids

A human DNA plasmid vector for overexpressing IGF1R (#RG214928) and Tyro3 (#SC108283) were purchased from Origene. pcDNA3 (#79020) was purchased from Invitrogen.

2.1.7.5 Antibodies

Tab. 11 Primary antibodies

Product	Species	Company
IGF1R	Rabbit	Cell Signaling Technology Inc., USA
Phospho-IGF-1-R	Rabbit	
TYRO3	Rabbit	
β–Actin	Mouse	Sigma-Aldrich, Germany

Tab. 12 Secondary antibodies

Product	Company
Polyclonal Goat anti-Rabbit	Dako GmbH, Germany
Polyclonal Rabbit anti-Mouse	
Polyclonal Mouse anti-Goat	Santa Cruz Biotechnologies, USA

2.2 Clinical patient data and tissues

Clinical data were used with informed consent of the patients and were generated in the participating institutions. Tumors were classified according to the current WHO classification of tumors of the thymus[11]. Histological tumor stage was assessed according to the modified Masaoka-Koga classification[56]. Native samples of the tumors in available cases were snap frozen in liquid nitrogen and stored at -80°C until further processing.

44 cases of malignant TH and TC were included in the study (21 male, 17 female and 6 unknown). The ages ranged from 36 to 78 years (median 54 years). The ages of 10 patients was uncertain. The specimens were obtained between 1986 and 2017. Two patients were diagnosed as Masaoka-Koga stage I, 5 patients as stage II, 9 patients as stage III and 16 patients as stage IV. In 12 patients, the Masaoka-Koga stage was not available. The specimens consisted of type B1 (1), type B2 (26), type B3 (4) and TC (13). MAPK arrays were performed with type B2 (8), type B3 (3) and TC (3). RTK

arrays were performed on 33 samples (type B1 (1), type B2 (20), type B3 (3) and TC (9)) and Pamgene arrays were performed on type B2 (11), and TC (6). The clinical

Tab 13: Patient samples

Patient Nr.	SEX	TH/TC	Diagnosis	Tumor	MG	Masaoka	Survival	Surviver	Recurrent	Age	RTK array	MAPK array	Pamgene
1	m	TC	TSCC	primary	no	4b	82	yes		69	no	yes	yes
2	m	TH	B2,5	primary	yes	4a	156	yes	yes	66	yes	yes	no
3	f	TC	Typ C	primary		3	132	no		57	yes	yes	yes
4	m	TC	TSCC	primary	no	2				63	yes	yes	no
5	m	TH	B3	primary	no	3	36	yes		61	yes	yes	no
6	m	TH	B2,5	primary		4b	55	no		58	yes	yes	yes
7	f	TH	B2	primary		3				47	yes	yes	yes
8	f	TH	B3	recurrence					yes	57	yes	yes	no
9	f	TH	B2	metastasis		4a				41	yes	yes	no
10	f	TH	B3	recurrence		3	192	yes	yes	47	yes	yes	no
11	m	TH	B2	primary		4a					yes	yes	no
12	m	TC	TSCC	primary		4b	60	yes			yes	yes	no
13	m	TH	B2	primary					yes	46	yes	yes	no
14	f	TH	B2	primary		4a				36	yes	no	yes
15	m	TH	B2	primary		4a	0			52	yes	yes	no
16	f	TH	B2,5	primary	yes	3	240	yes		51	yes	no	yes
17	m	TH	B1,5	primary	no	2				51	yes	no	yes
18	f	TC	TSCC	primary	no	3	132	no		57	yes	no	yes
19	m	TH	B2	primary	yes	3	47	no		53	yes	no	no
20	f	TC	Typ C	primary		4	12	yes		45	yes	no	no
21	m	TH	B2	primary	no	2	108	no		57	yes	no	no
22	m	TH	B2	primary	yes	4a	57	yes	yes	43	no	no	no
23	m	TH	B2	primary		1	224	yes		47	yes	no	no
24	f	TH	B2,5	primary	yes	2	12	yes		71	yes	no	yes
25	m	TH	B2	primary	no	2					no	no	yes
26		TC	Typ C	primary		3	36	no			yes	no	no
27	f	TH	B2	recurrence					yes	73	yes	no	yes
28	m	TH	B2	metastasis		4a	53	yes	yes	78	yes	no	no
29	m	TC	Typ C	metastasis					yes		yes	no	no
30		TH	B3	primary							no	no	yes
31	f	TH	B2,5	primary		4b	53	yes		69	yes	no	no
32	f	TH	B2	primary	yes	1	0			38	yes	no	yes
33	m	TH	B2	primary		4a	0			47	yes	no	no
34	f	TH	B2,5	primary	no					60	yes	no	no
35	m	TC	TSCC	primary						70	yes	no	no
36	f	TC	B3/C	primary		3	0			60	yes	no	no
37	f	TH	B2	primary						56	yes	no	no
38	m	TH	B2,5	primary		4a	0			45	yes	no	yes
39		TC	Typ C	primary							no	no	yes
40		TH	B2	primary							no	no	yes
41		TC	Typ C	primary							no	no	yes
42		TC	Typ C	primary							no	no	yes
43	m	TH	B2,5	metastasis	no	4a				30			yes
44	f	TH	B2	metastasis	no	4a				41			yes

TSCC, thymic squamous cell carcinoma; B2,5, B2/B3; B1,5, B1/B2; Survival: month

patient data of the tissue array subjects are shown in Table 2. (see 3.2.4.1 and 3.2.5.1). The study was approved by the ethics committee of the Medical Faculty Mannheim, University of Heidelberg (2013-802R-MA) and University Medical Center Göttingen (GÖ 912/15).

2.3   Methods

2.3.1 Cell culture and resistance development

The thymoma cell line TAB1, the thymic carcinoma cell line 1889c, the prostate cancer cell line PC3, the breast cancer cell line MCF7 and the colon adenocarcinoma cell lines HCT116 and HT29 were cultured in 1650 RPMI with 10% FCS and 1% L-glutamine. The renal carcinoma cell lines Caki2 and Caki1 were cultivated in McCoys medium with 10% FCS, 1% L-glutamine and essential amino acids. All cells were cultured with 1% penicillin / streptomycin. All cells were cultivated at 37°C in a 5% CO_2 atmosphere in a humidified incubator. For the generation of sunitinib resistance, TAB1 and Caki2 were subjected to increasing concentrations of sunitinib over 6 to 8 weeks, from 0.5 to 5 µM, by a stepwise 0.5 µM increase. Starting with 0.5 µM, cells were cultured until cell growth was equal to that of wild type control. Then the sunitinib concentration was increased by 0.5 µM. Resistance was monitored using an MTS test with 5 µM sunitinib against the WT control over 48 h (see section 2.3.2).

2.3.2 Cell viability analysis (MTS)

Cell viability was measured using the CellTiter 96® AQueous One Solution Cell Proliferation Assay (Promega Corporation). This assay is a colorimetric approach based on the activity of the cellular mitochondrial reductase in metabolically active cells. The yellow-colored tetrazolium compound of the MTS reagent (3-(4,5-dimethyl-2-yl)-5-(3-carboxymethoxyphenyl)-2-(4-sulfophenyl)-2H-tetrazolium) is reduced to purple formazan in the presence of active mitochondria. The absorbance of the purple color can be measured and thus allows a conclusion about the viability of the cell. To measure cell viability, equal numbers of cells (e.g. 5,000 – 10,000) were seeded in six replicates for each treatment into 96-well flat-bottom plates. Cells attached overnight and were subsequently incubated for 48 hours with 5 µM sunitinib. 20 µl MTS reagent was added to each well and samples were incubated for 1-3 hours at 37°C. Cell viability was determined by measuring the absorbance at 490 nm and reference 655 nm using i-control on the Tecan Infinite M200PRO plate reader. The impact of sunitinib on cells was calculated by normalizing each value by the mean of the untreated control replicates. Relative viability was plotted as a bar graph and significance of treated samples were calculated to control using a student t-test.

2.3.3 Preparation of cell and tissue lysates for Western blot

Proteins were isolated from cell cultures and fresh frozen human tissue samples. Cells were generally cultured in a 6-well format for protein isolation (see 2.3.1). They were then washed with 1 ml PBS and lysed by adding 65 µl protein lyses buffer. The cells were scratched off using a cell scraper, the lysate was transferred to an Eppendorf cup and then incubated on ice for 30 min. The lysate was centrifuged at 4°C for 30 min at 14,000 rpm and the protein lysate was transferred into a new tube. For protein isolation from human tissue samples, frozen tissue was sliced in 5 µm sections and 5 slices were re-suspended and partially homogenized in 100 µl lysis buffer by repeated up and down pipetting. Samples were incubated on ice for 30 min and subsequently centrifuged for 30 min at 4°C at 14,000 rpm, and the protein lysate was transferred into a new tube. All protein lysates were stored at -80°C until further use.

2.3.4 Protein extraction and screening for activated RTKs and MAPK

Protein lysates for the Proteome Profiler^{TM} Array (Human Phospho-RTK Array Kit) and the Human Phospho-MAPK Array Kit were prepared according to the manufacturer's protocol. 1 x 10^7 cells collected by trypsinization from a 75 cm^2 flask were washed with PBS and the remaining PBS was removed before 1 ml lysis buffer (1 ml lysis buffer 17 with 10 µg/mL aprotinin, 10 µg/mL leupeptin, and 10 µg/mL pepstatin) was added. The cell pellet was re-suspended and lysed by pipetting up and down and rocking the lysates gently at 2-8 °C for 30 minutes. The samples were centrifuged at 14,000 x g for 5 minutes and the supernatant was transferred into a clean tube. Whole tumor tissue lysates were prepared from 15 5 µm-thick sections. Lysates were then snap frozen in liquid nitrogen and stored at -80°C until further use.
For the detection of phosphorylated kinases, membranes were blocked and 250 µg of protein lysate was incubated at 4°C overnight on the specific array. The membranes were washed twice with wash buffer before incubating with an anti-phospho-tyrosine-HRP detection antibody for 2 hours at RT. For imaging, the Chemiluminescent Detection Reagent from the Array Kit was mixed in ratio 1:1. After two additional wash steps,the membrane was incubated for 1 min with 1 ml of the reagent mix and imaging was done performed using the Fusion FX7 chemiluminescence detection system. The "signal intensity" was analyzed using the software ImageJ V1.51 (NIH, Maryland, USA) followed by normalization to the reference spot of the membrane.

2.3.5 Preparation of cell and tissue lysates for kinase array

About $3*10^5$ cells were collected by trypsinization in general from a 6-well dish and cells were pelleted by centrifugation for 5 min at 800 g and 4°C. For fresh frozen tissue, five 10-micron frozen sections were collected from TH and TC patient samples. Proteins were extracted in 100 µl ice-cold M-Per lysis buffer (Thermo Fisher Pierce, Rockford, IL, USA) containing 1:100 Halt's protease and phosphatase inhibitors (Pierce cats. 78420, 78415, Thermo Fisher Pierce, Rockford, IL, USA). Samples were re-uspended in lysis buffer, incubated on ice for 15 min and centrifuged at 14,000 rpm for 15 min at 4°C. The supernatant was aliquoted and stored at –80°C.

2.3.6 Protein lysate quantification

Two different methods to quantify proteins were applied. For lysates containing SDS, the Pierce 660nm protein assay reagent (Thermo Fisher Pierce, Rockford, IL, USA) was used, for RIPA protein lysates the DC^{TM} protein assay kit (BioRad). Protein concentration quantified with the Pierce 660 nm protein assay reagent were calculated according to the Pierce™ bovine serum albumin standard pre-diluted set (Thermo Fisher Pierce, Rockford, IL, USA). 5 µl protein sample and diluted standard was pipetted in duplicates in a 96-well dish. 75 µl of protein assay reagent was added to each sample, mixed and incubated for 5 min at RT. The absorbance was measured at 660 nm using the Tecan reader. The sample protein concentrations were calculated according to the formula generated by the linear regression of the diluted standards. Protein concentrations of RIPA whole lysates were quantified in a colorimetric Lowry assay using the DC^{TM} protein assay kit (BioRad) adjusted to small volumes of protein lysate. In this assay, the solution S was diluted 1:50 in solution A. 20 µl of this mixture was added to 2 µl of the protein sample in a 96-well plate (Greiner Bio-one) before 200 µl of solution B was added. Absorbance of each sample was measured in triplicate at 700 nm using the Tecan Infinite M200PRO plate reader (Tecan) with the corresponding software Magellan 7.1. The software calculated the median of triplicates and the protein concentrations based on a deposited standard curve algorithm.

2.3.7 Multiplex profiling of protein tyrosine kinase substrates

1 µg of cell lysate and 5 µg of tissue lysate were prepared in 40 µl of a final volume of kinase master mix containing the kinase assay buffer (50 mM Tris-HCl pH 7.5, 10 mM MgCl2, 1mM EGTA, 2 mM dithiothreitol, 0.01% Brij 35, 1 mg/ml BSA, 12.5 µg/ml FITC-labelled PY-20 antibody and 0.4mM ATP) in accordance with the instructions provided by the manufacturer (PamGene, 's-Hertogenbosch, The Netherlands). Each sample was measured as DMSO control and conducted with 5 µM sunitinib. Profiling of the substrate tyrosine phosphorylation from cell lines, malignant TH and TC protein lysates was performed with PTK PamChip®4 microarrays on a PamStation®12 (PamGene, 's-Hertogenbosch, The Netherlands) at 30°C. The software Evolve (PamGene, 's-Hertogenbosch, The Netherlands) was used for initial sample and array processing as well as image capture. Tyrosine phosphorylation was followed over 64 cycles.

2.3.8 Image filtering, data adaptation and SRI prediction model generation

For sample and array annotation, image gridding, quality control (QC) and for phosphorylation-signal quantitation the software package BioNavigatoR (version 6.2; PamGene, 's-Hertogenbosch, The Netherlands) were used. Annotated data packages were stored in the repository in a project-specific order. The slope of the peptide signal intensity across different exposure times (10, 20, 50,100, 200 ms) was multiplied by 100 and log2-transformed. The resulting per spot value was used for further analyses. The sunitinib inhibition was defined as the log2 ratio of the signal obtained for the same sample treated and non-treated with 5 uM sunitinib. The inhibition ratios were used for all subsequent calculations for generating the prediction quantifier, two-group comparison and cell and tissue response prediction[57]. The prediction classifier was established using PLS-DA [58-60], resulting in a sunitinib response-prediction index (SRI).

2.3.9 Upstream kinase prediction

To predict kinases involved in the sunitinib resistance, significant values of a two-group comparative analysis between resistant and non-resistant samples (quantifier, cells and tissue) was performed and the significant single values were visualized by a heat map. The significant tyrosine phosphorylation sites were subjected to upstream kinase

prediction using the upstream kinase operator. This operator within the Bionavigator software maps peptides using standard BLAST tools to match the peptides on the chip to phosphor sites in the human proteome. The phosphoNET database (www.phosphonet.ca) queries kinases that are predicted to phosphorylate these sites. Comparing two experimental groups, this information is added to the included peptides by enrichment. A significance score Qsp is calculated, including the significance of the multiple kinase-associated statistic values (www.phosphonet.ca) The final score Q is used to rank the included kinases for putative involvement in the observed experimental differences. The top values from the specificity and sensitivity scores were considered for further investigation.

2.3.10 Western blot

WB was performed with 15 µg protein in 4x Laemmli sample buffer (BioRad) containing β-mercaptoethanol for denaturation. Samples were denatured at 95°C for 5 min and cooled down on ice. Single samples together with a protein ladder (Thermo Fisher Scientific) were loaded onto a precast Mini Protein TGX gel (BioRad) in a gel chamber with TGS running buffer (BioRad). Protein was stacked at 80 V for 5 min and run at 250 V. The run was stopped when the blue loading dye reached the end of the gel. Proteins were transferred onto a nitrocellulose membrane using the Transfer Kit and the semi-dry Trans-Blot Turbo^{TM} System (BioRad) with the corresponding programs. After blotting the membrane was washed in TBST and the protein transfer was visualized by staining the membrane with Ponceau S solution. This dye has a light red color that can be used for a rapid reversible detection of protein bands. To avoid unspecific binding reactions of the primary antibody the membrane was blocked in 5% milk in TBST for 1 h at RT. The membrane was then rinsed with TBST and incubated overnight with the primary antibody (Tab. 9) diluted in TBST at 4°C. The membrane was subsequently washed three times with TBST and incubated with an appropriate secondary antibody (Tab. 10) diluted in TBST for 1 h at RT. The membrane was then again washed three times in TBST and covered with an appropriate volume of the peroxidase substrate Western Lightning Plus ECL Prime (Perkin Elmer Inc.). Proteins were detected using the Fusion FX7 chemiluminescence detection system (Peqlab). β-Actin was applied as a loading control in each WB experiment performed. ImageJ was used to quantify protein signal intensities.

2.3.11 Vector amplification

Chemically competent Subcloning Efficiency™ DH5α™ was used to amplify DNA plasmids. 25 ng of plasmid DNA, in less than 5 µl H_2O, was incubated in 50 µl bacterial cell suspension on ice for 30 min. The bacteria were heat shocked at 42°C for 30 sec and then placed directly on ice for 2 min. They were then subjected to 1 ml LB medium and incubated at 37°C and 450rpm for 1 h in order to recover. The bacteria were then added to 50 ml LB medium containing 100 µg/ml ampicillin for selection and overnight (16 hours) culture in a 37°C incubator shaking at 225 rpm. A QIAGEN Plasmid Midi Kit® was used for enriched plasmid isolation following manufacturer's instructions. The bacteria were harvested by centrifugation at 6000 g for 15min. The pellet was re-suspended, lysed and the protein was precipitated. The lysate was filtered using a Whatman filter and the supernatant was applied to an equilibrated Qiagen-tip 500 column. After two washing steps, the plasmid DNA was eluted, precipitated in isopropyl and centrifuged at 10000 g for 15 min. The pellet was then washed twice in 70% EtOH and centrifuged before being air-dried and re-suspended in 8 0µl RNase-free water. Plasmid DNA was quantified using the NanoDrop before samples were stored at -20°C.

2.3.12 Knockdown of IGF1-R and TYRO3/DTK using siRNA

Cells were transfected with 80 nM siRNA against either IGF1-R (Hs_IGF1R_7, catalog. No. SI02624552) or TYRO3/DTK (Hs_TYRO3_5, catalog No. SI00288344; Qiagen) using HiPerFect Transfection Reagent (Qiagen) according to the manufacturer's protocol. Briefly, 100 µl transfection medium containing 12 µl HiPerFect, 9.6 µl siRNA/negative control (20mmol/L), and 78.4 µl RPMI160 medium without FCS was incubated at room temperature for 20 min and added to $3*10^5$ cells in 2.3-mLmedium just after seeding. Cells were incubated for 24 hours and further processed for immunoblot and viability assay.

2.3.13 Transfection and overexpression of TYRO3/DTK and IGF1R

TAB1, 1889c and Caki2 were transfected in 96-well and in 6-well cell culture plates (see 3.2.3.1). 100 µl transfection mix was prepared using FCS-free RPMI-1640 medium, 2 µg of the DNA plasmid and 2 µl X-treme GENE HP DNA Transfection Reagent (Roche). The mix was vortexed and incubated for 20 min at RT before it was added dropwise to freshly seeded cells using 5 µl/well for 96-well and 100 µl/well for 6-well cell culture plates. Cells were incubated at 37°C and 5% CO_2 concentration. Overall, cells were incubated up to 96 h with or without sunitinib treatment (see 3.2.3.3) according to the experimental setting.

2.3.14 Reconstitution of IGF1-R and TYRO3/DTK

Cells were transfected with 1 µg expression vector TYRO3/DTK /Dtk (CAT#: SC108283, Origene) or IGF1R (CAT#: RC600009, Origene) using X-tremeGENE™ HP DNA Transfection Reagent (Roche) according to the manufacturer's protocol. Briefly, 100 µl transfection medium containing 1 µg of plasmid DNA 98 µl RPMI160 medium without FCS and 1 µl X- tremeGENE was incubated at room temperature for 20 minutes and added to $3*10^5$ cells. Cells were incubated for 24 hours before sunitinib treatment and further processed for immunoblot or viability assay.

2.3.15 Statistical analysis and data presentation

Statistical analysis was performed using GraphPad Prism 7.0d for Mac. Significant differences between two groups were calculated using either student's t-test or the Mann-Whitney U test depending on normality of signal distribution, which was assessed by the Shapiro-Wilk test. Multiple t-tests were performed using One-way ANOVA. Bivariate correlations were carried out using Pearson (for continuous variables) or Spearman (for ordinal variables) correlation coefficients. Data are presented as mean ± standard error of the mean (SEM), unless otherwise stated. Significance values are stated as follows: p $\leq$ 0,05 (*), p $\leq$ 0,005 (**), p $\leq$ 0,0005 (***).

3 RESULTS

3.1 Phospho RTK and MAPK arrays of malignant TH and TC

An earlier clinical study found that patients responding to sunitinib activate certain RTKs, including epithelial growth factor receptor (EGFR), insulin receptor (IR), RET proto-oncogene, IGF-1R and TYRO3/Dtk[38]. Other groups have shown that IGF-1R is increased in TC[61], and IGF-1R inhibitors have been implicated in clinical trials for TH and TC treatment[62]. Therefore, we first tested the activity of RTKs and MAPKs in malignant TH or TC patient samples. We applied tissue lysates from 33 patients on phospho RTK arrays and from 14 patients on MAPK arrays as described in Material and Methods (Table 1). The arrays were scanned, signals were background corrected and normalized to positive controls (Supplement Table 1 and 2). First, we looked at the signal distribution of single RTKs in all patients and then sorted out the single RTK phospho signals throughout all samples by their intensity. For almost all RTKs, at least
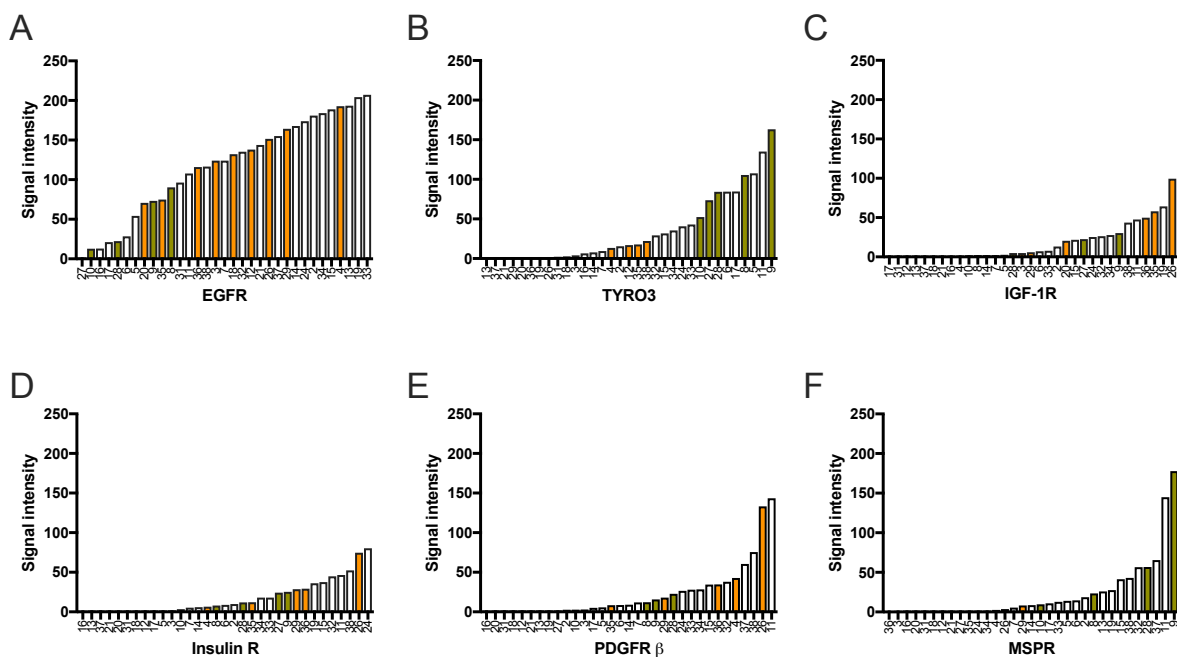

Figure 3: Phospho signals and distribution of prominent RTKs in malignant TH and TC. Distribution of single phospho signals of EGFR (A), TYRO3/Dtk (B), IGF-1R (C), IR (D), PDGFRβ (E) and MSPR (F) sorted by intensity. Orange bars mark TC. Olive bars mark recurrent or metastatic TH. TH = 24, TC = 9. The distribution of all single RTKs is shown in Supplemental Figure 1.

one single strong signal was observed in one of the tissue samples (supplemental Figure 1), but the RTK activation was heterogeneous in the tumor cohort. The most prominent RTKs with a wider range of moderately activated RTKs included pEGFR, pTYRO3/Dtk, pIGF-1R, pIR, pPDGFR β and pMSPR (Figure 3A-E). The strongest signals were detected for pEGFR, which was present in almost all samples. TC (orange bars) showed moderate to strong RTK activation in the six shown samples. In contrast, recurrent and metastatic TH (olive bars) showed a strong activation of TYRO3/Dtk and MSPR and less activation of EGFR.

3.2 Hierarchical clustering of RTK arrays

To investigate whether there are subgroups with specific RTK activation within the present cohort of TH and TC, we applied an unsupervised hierarchical clustering using Morpheus (https://software.broadinstitute.org/morpheus). Data were adjusted by quantile normalization and columns and rows were clustered by the average linkage method. This resulted in two heterogenous groups that were predominantly defined by pEGFR and pTYRO3/Dtk (Figure 4, top). We then took the mean phospho signals of
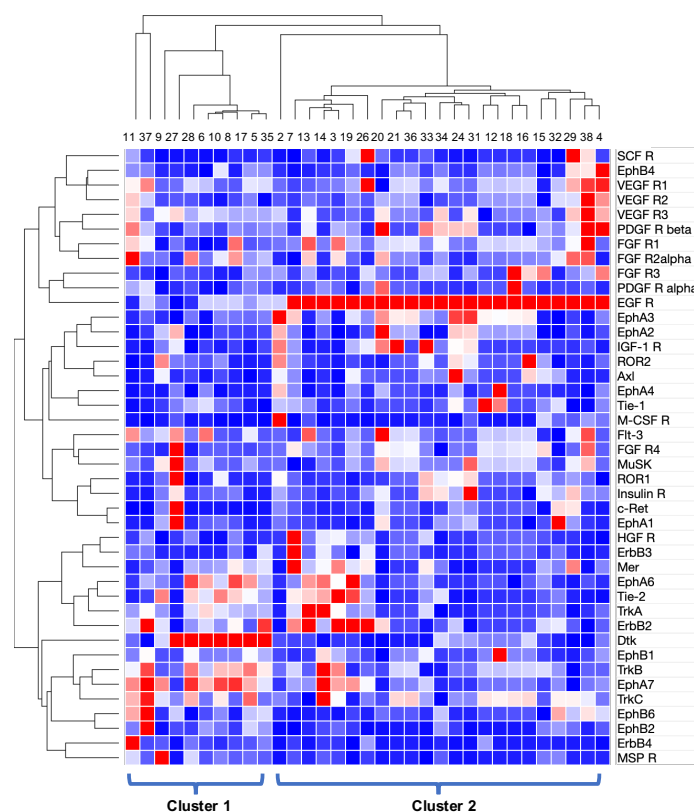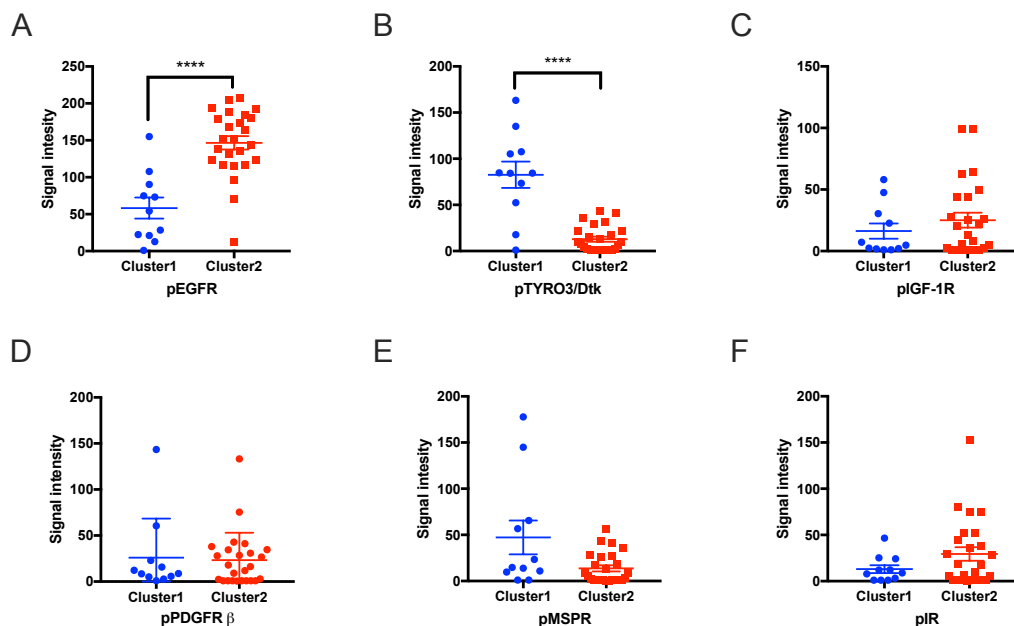
Figure 4: Hierarchical clustering of RTK phosphoarrays and analysis of subgroups of activated RTKs. Upper panel: Hierarchical clustering patient samples indicated two groups (Cluster 1 and 2) of differentially activated RTKs. Lower panel: Cluster comparison of the most dominant RTKs pEGFR (A), pTYRO3/Dtk (B), pIGF-1R (C), pPDGFRβ (D), pMSPR (E) and pIR (F). (n = 33)

a specific RTK and compared the clusters to each other. Using student's t-test, of the 6 predominant RTKs a statistically significant difference between clusters 1 and 2 could only be shown for EGFR and pTYRO3/Dtk (Figure 4 A-F). IR, pPDGFR and pMSPR did not show a difference in activation.

To investigate whether the significantly different activity of EGFR and pTYRO3/Dtk also correlated to recurrent or metastasized TH (Figure 1), we compared them to
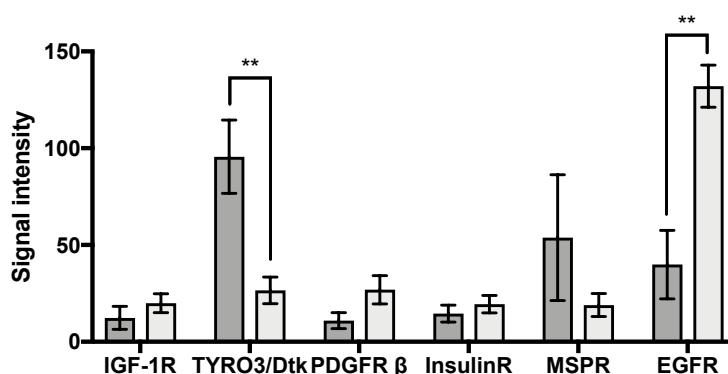

Figure 5: Comparison of RTK activity of recurrent and metastatic TH with primary TH and TC Comparison of the activity of recurrent/metastatic (dark grey bars) and primary tumors (light grey bars) shows a significant difference in activity of TYRO3/Dtk and EGFR (G). Relative phosphorylation is represented by the "Signal Intensity" as described in Material and Methods.

primary TH and TC. This showed that pTYRO3/Dtk was significantly more activated in recurrent and metastatic TH, whereas EGFR activity was significantly increased in primary tumors. However, pIGF-1R, pPDGFRβ, pMSPR and pIR did not show any significant differences (Figure 5).

3.3 MAPK arrays of 14 malignant TH and TC

Due to the limited number of tissue samples, we were only able to performed MAPK arrays in 14 samples according to the RTK arrays (Table 1and Figure 6A). The mean phospho values of the MAPK were higher than those of the RTKs (Figure 6B). Hierarchical clustering resulted in 2 major groups with 3 distinct clusters (clusters 1-3)
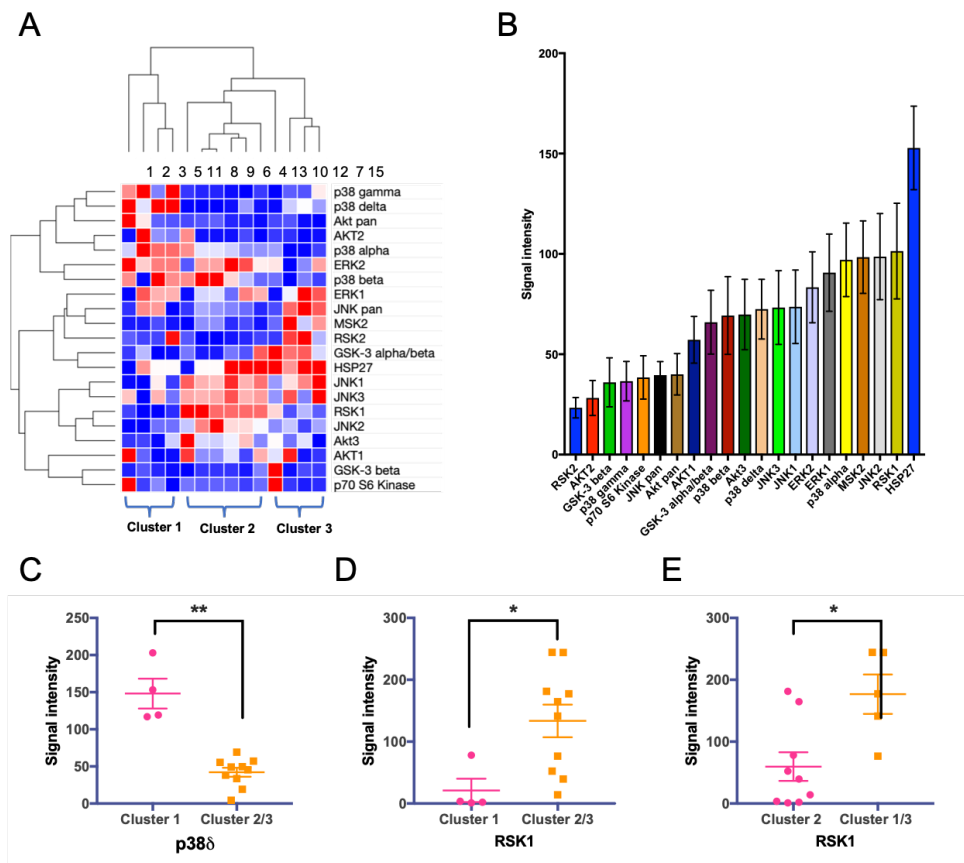
Figure 6: Hierarchical clustering MAPK arrays to predict differentially activated groups. Hierarchical clustering of phospho MAPK signals of patient samples resulted in three groups (clusters 1, 2 and 3) (A). The mean MAPK activation was higher than the RTK signals, with RSK2 showing the lowest and HSP27 the highest signals (B). Comparison of MAPK activity within the clusters. p38δ and RSK1 in cluster 1 vs 2/3 (C and D) and RSK1 in cluster 2 vs 1/3.

(Figure 6A). Comparison of the two main clusters (cluster 1 vs. cluster 2/3) revealed a significantly different activity of p38δ and RSK1. Cluster 1 showed a significantly stronger activation of p38δ and decreased RSK1 activation (Figure 6C and D). RSK1 was also significantly less activated in cluster 2 (Figure 6E).

3.4 Analysis of clinical data

To test whether any RTK was related to other available clinical parameters, we compared the phospho signals of all RTKs to histological tumor type, MG status and Masaoka-Koga stage (Table 1). Do to the rather small groups for the specific comparisons this did not reveal any significant differences or correlations.

3.5 Cell lines with different sunitinib response

To establish an in vitro assay for sunitinib resistance, we then used the TH cell line TAB1, the TC cell line 1889c, the breast cell line MCF7[63], and the colon cancer cell lines HT29[64] and HCT116[65] with published responses to sunitinib. Cells were treated with different concentrations (0, 2, 5 and 10 uM) of sunitinib over 120 hours (Figure 7). This revealed different growth patterns for each cell line. TAB1 was the least resistant cell line with a significant difference in growth for 5μM sunitinib already after 24 hours, in contrast to the other cell lines with no significant response until after 48 hours (Figure 7A and C). 1889c, HTC116 and MCF7 did not develop a significant response to 5 μM sunitinib until 72 hours treatment (Figure 7A, D and E). MCF7 seemed to be the most resistant cell line even when grown under 10μM sunitinib treatment. Therefore, 5 μM sunitinib treatment for 48 hours was used for further experiments.

3.6 Drug dosage and resistance induction of TAB1 and Caki2

Since TAB1 was the only sunitinib-responsive cell line, there was need of a second non-resistant cell line. Recurrent renal cell carcinomas (RCC) are also treated with sunitinib as second-line therapy[66], and thus RCC cell lines Caki1 and Caki2 were tested for sunitinib response. After treating 1889c, TAB1, Caki1 and Caki2 cells with 5 μM sunitinib for 48 hours, cell growth was significantly reduced in TAB1 and Caki2,
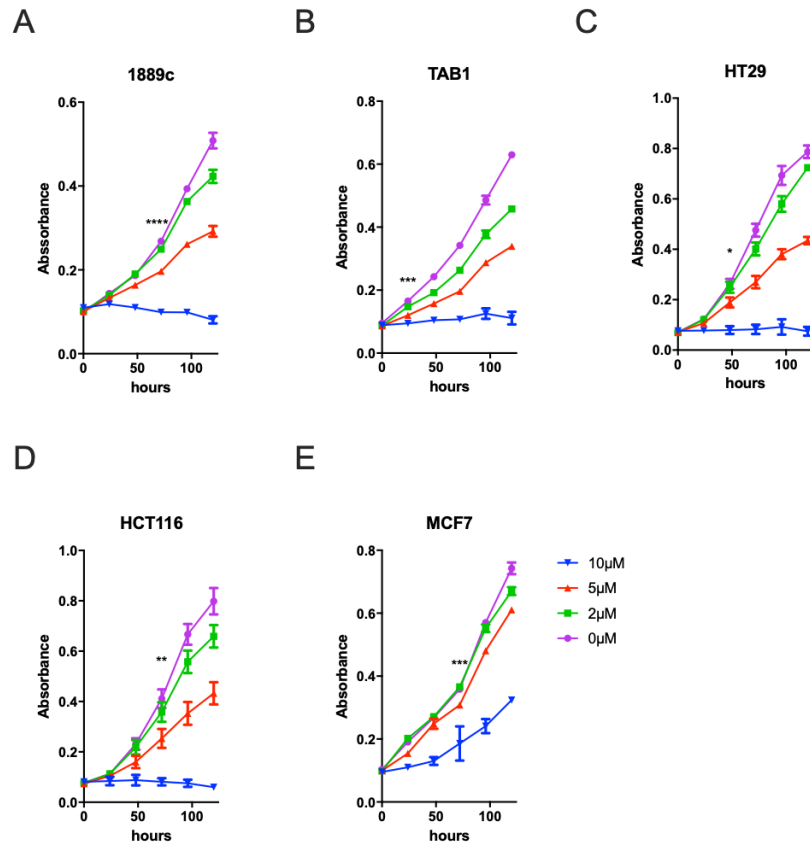
Figure 7: Sunitinib treatment of different cancer cell lines over 120 hours. The cell lines 1889c (A), TAB1 (B), HT29 (C), HCT116 (D) and MCF7 (E) were tested in terms of their response to different concentrations of sunitinib (0, 2, 5 and 10μM) using MTS viability assay. Responses were monitored every 24 hours up to 120 hours. Asterisks indicate the earliest time point when a significant difference was detected with 5μM sunitinib. (n=6)

whereas 1889c and Caki1 showed no difference in viability in comparison to untreated controls (Figure 8A). To induce resistance to sunitinib, TAB1 (TAB1R) and Caki2 (Caki2R) cells were cultured under increasing sunitinib concentrations (0.5 to 5 μM) as described in Material and Methods. Cells were cultured until a steady growth and normal viability was detectable before increasing the sunitinib concentration. Resistance induced cell lines TAB1R and Caki2R showed a significant difference to native TAB1and Caki2 and an almost equal viability as the resistant cell line 1889c and Caki-1 (Figure 8B).

3.7 Generation of the sunitinib response index (SRI)

To predict sunitinib response in patient samples, we generated an index of sunitinib response (SRI). For this, we measured TAB1, TAB1R, Caki2 and Caki2R in the presence or absence of sunitinib, and to assure equal QC and prediction classifier conditions, all measured samples including resistance induced cell lines, native cell lines and tissue samples were implemented. Before the sunitinib-DMSO ratio was generated, phospho signals of separate sunitinib-treated and DMSO controls were visualized (see Supplementary Figure 2A and B, respectively). Visualization and unsupervised clustering of the ratio values showed a clear grouping (Supplemental Figure 2C). Ratios and inhibition profiles were obtained as described in the Material and Methods section. Four resistance-induced, 2 TAB1R and 2 Caki2R as well as four
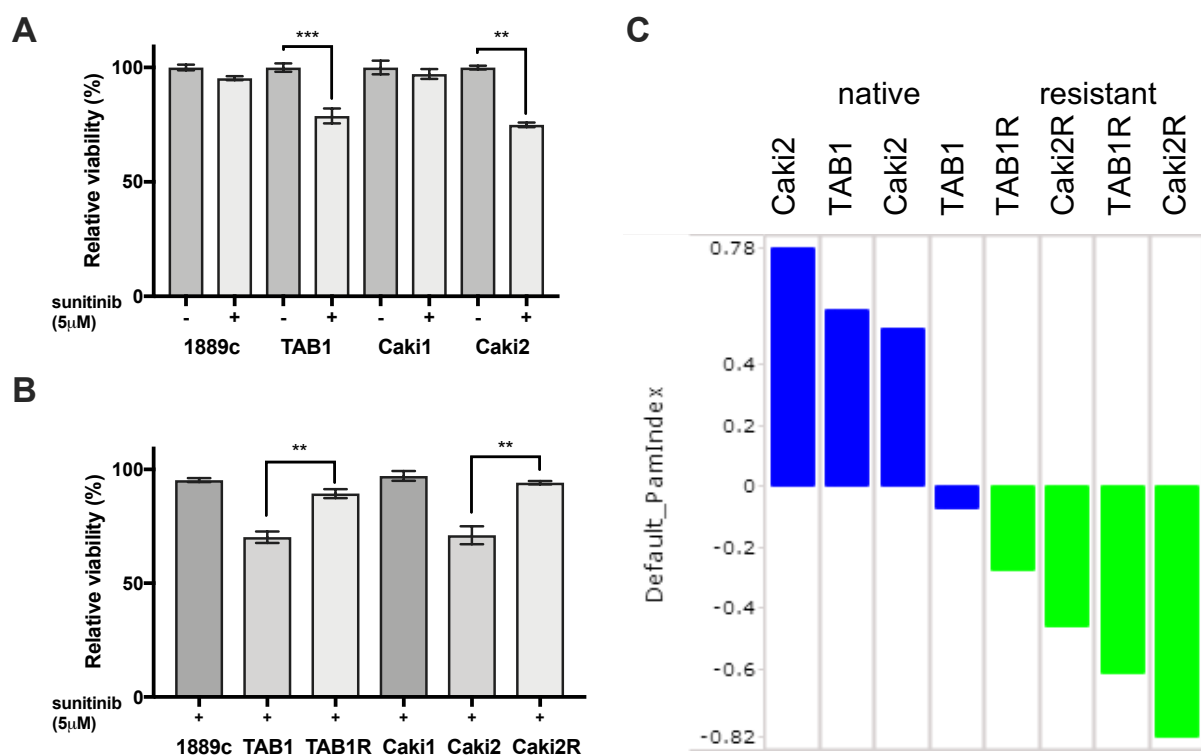
Figure 8: Induction of sunitinib resistance in TAB1 and Caki2 and generation of sunitinib response index (SRI). TAB1 and Caki2 showed a 20% decreased viability after 5 µM sunitinib treatment over 48 hours as compared to 1889c and Caki1. (N= 6) (A). Sunitinib resistance induced TAB1R and Caki2R after 5 µM sunitinib treatment for 48 h (N= 6) (B). Visualization of the prediction quantifier with generated Pam index (SRI) from 4 native and 4 sunitinib resistance-induced cell lines (C).

corresponding native cell lines were selected to generate the SRI using the prediction classifier as described in Material and Methods. This resulted in a prediction classifier as shown in Figure 8C.

3.8 Validation of SRI in cell lines

To validate the SRI, we first tested TAB1, TAB1R, Caki2, Caki2R, 1889c, Caki1, PC3, HT29 and HCT116 for their response to 5μM sunitinib after 48h by MTS, and then separated the cells according to their relative viability in a responding (orange bars) and a resistant group (olive bars) (Figure 9A). The application of the SRI resulted in a

A
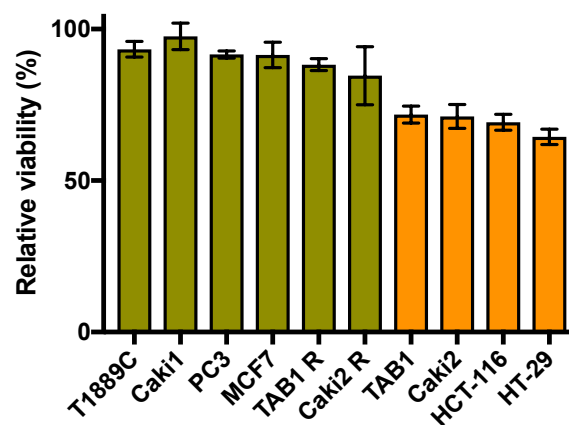
B
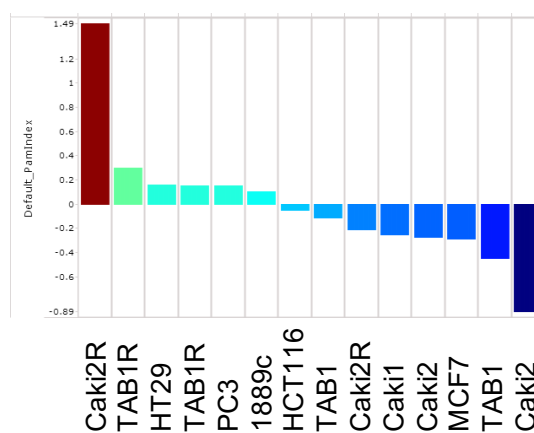
Figure 9: Validation of SRI on cell lines. Tested cell lines were plotted according to their relative viability after sunitinib treatment in comparison to untreated controls. Responsive cell lines are orange, resistant olive green (N=6) (A). Representation and order of the SRI of cell lines in A. Positive SRI values represent resistance and negative SRIs predicted native cells (B).

separation of the cell line in two groups, with different indexes. The SRI accurately re-estimated the resistance-induced cell lines by mistaking one Caki2R. In addition, the SRI predicted PC3, 1889c and HCT116 accurately and mis-predicted Caki1, MCF7 and HT29. These results indicate that the SRI may predict sunitinib resistance to a certain degree, but there may be other mechanisms that influence the response to sunitinib (Figure 9B). Nevertheless, we performed a hierarchical clustering and an upstream kinase prediction of the two predicted groups as described in Material and Methods. The top 10 predicted scores were for FLT1, FMS, BRK, FYN, TYRO3/Dtk KDR, BMX, TEC, PYK2 and VEGFR3 as predicted kinases (Supplemental Figure 3 and 4).

3.9 SRI application on tissue samples and upstream kinase prediction

The *in vitro* SRI (developed in cell lines) was also applied to 17 malignant TH and TC. This resulted in two distinct clusters with potentially responding patients (negative values) and a second putative resistant group (positive values) (Figure 10). Importantly, one sample came from a patient with TC and liver metastases (pre-
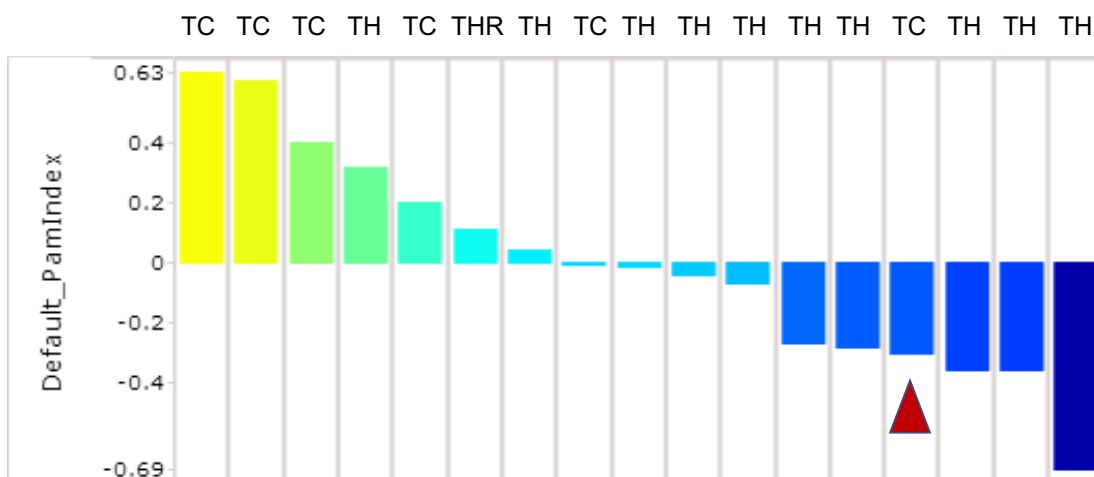
Figure 10: Waterfall plot of SRI prediction of sunitinib response in 17 malignant TH and TC samples. The application of the SRI to tissue samples divided TH and TC into two distinct groups that can be considered possible responders (negative values) and non-responders (positive values). Bars are marked with the TH or TC (R = recurrent sample). Sunitinib-responding patient is marked with a red triangle.

therapeutic) who was known to have experienced a partial remission and stable disease under sunitinib treatment. This patient was predicted to be a potential responder (red triangle). The most probable kinases responsible for the difference between responders and non-responders in the upstream kinase prediction were FGFR1, ALK, TYRO3/DTK, ERBB3, BRK, TEC, PYK2, FGFR2, CTK and TRKB (Figure 11A and B, Supplemental Figure 5).
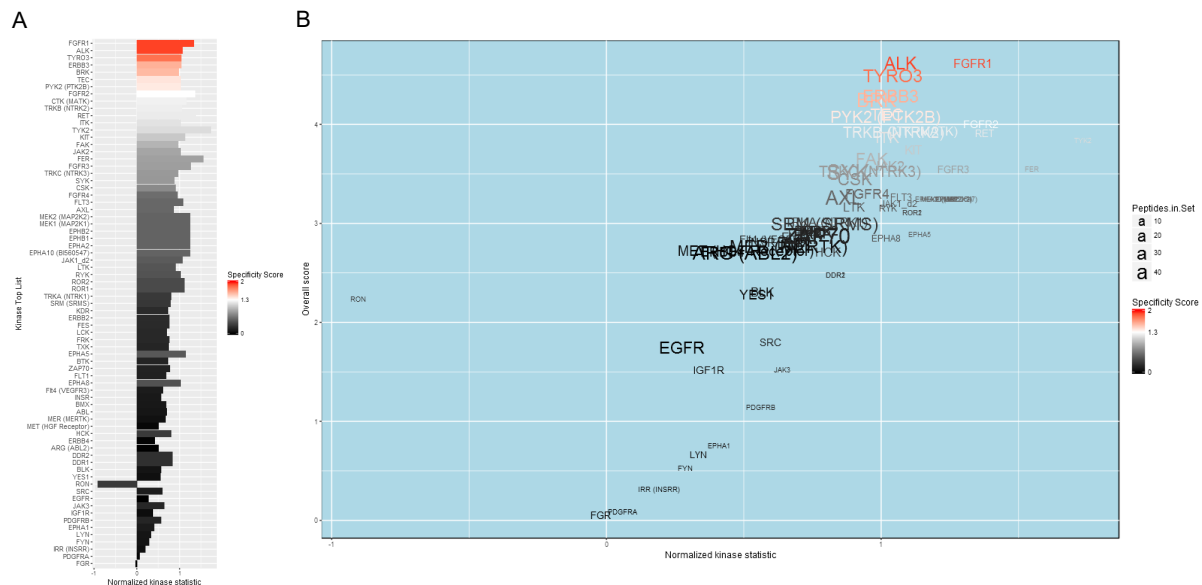
Figure 11: Upstream kinase prediction of potentially resistant and responsive patients. Inhibition values and specificity score of tissue lysates after SRI application (A). Vulcano plot of the upstream kinase prediction of tissue (B).

3.10 IGF1R and TYRO3/Dtk for functional testing

When comparing the upstream predictions of cell lines and tissues, TYRO3/Dtk was commonly predicted in the top 5 with a strong specificity score. TYRO3/Dtk has not been shown to be a target of sunitinib, but is activated in sunitinib-responsive patients[40]. However, since TYRO3/Dtk was one of the strongest activated RTKs with a significance increase in recurrent and metastatic patient samples, it received particular focus. IGF-1R was not among the top hits of the upstream kinase prediction, but results from earlier studies had shown an increased activity in sunitinib-responsive patients. Moreover, inhibition of IGF-1R has already been tested in small clinical trials[62]. IGF-1R is overexpressed in many TH and TC and is a potential target of

sunitinib[54]. Therefore, TYRO3 and IGF-1R were studied further for their relevance in the sunitinib response.

3.11 Expression of IGF1R and TYRO3/Dtk in native and resistant cell lines

We performed WB in lysates of native and resistant cell lines to detect IGF-1R and TYRO3/Dtk protein. IGF-1R protein expression was decreased in Caki1R and TAB1R but not in Caki2R in comparison to their parental cell lines. Treating Caki2R with 5 μM sunitinib even increased IGF-1R protein levels (Figure 13 A, upper panel). TYRO3/Dtk levels did not decrease in resistant cell lines in comparison to their native counterparts. However, treating resistant cell lines with 5 μM sunitinib almost abrogated TYRO3/Dtk signals (Figure 13 A, lower panel).

3.12 IGF-1R and TYRO3/Dtk influence sunitinib resistance in TC and TH cell lines

To evaluate on a functional level whether low levels of IGF1-R and/or TYRO3/Dtk are responsible for the resistance against sunitinib, we knocked down both genes with two independent siRNAs separately in the parental cell line TAB1 and Caki2 and subsequently treated them for 48 hours with 5 μM of sunitinib. In the case of IGF1R, the downregulation in the susceptible parental cell lines significantly increased the
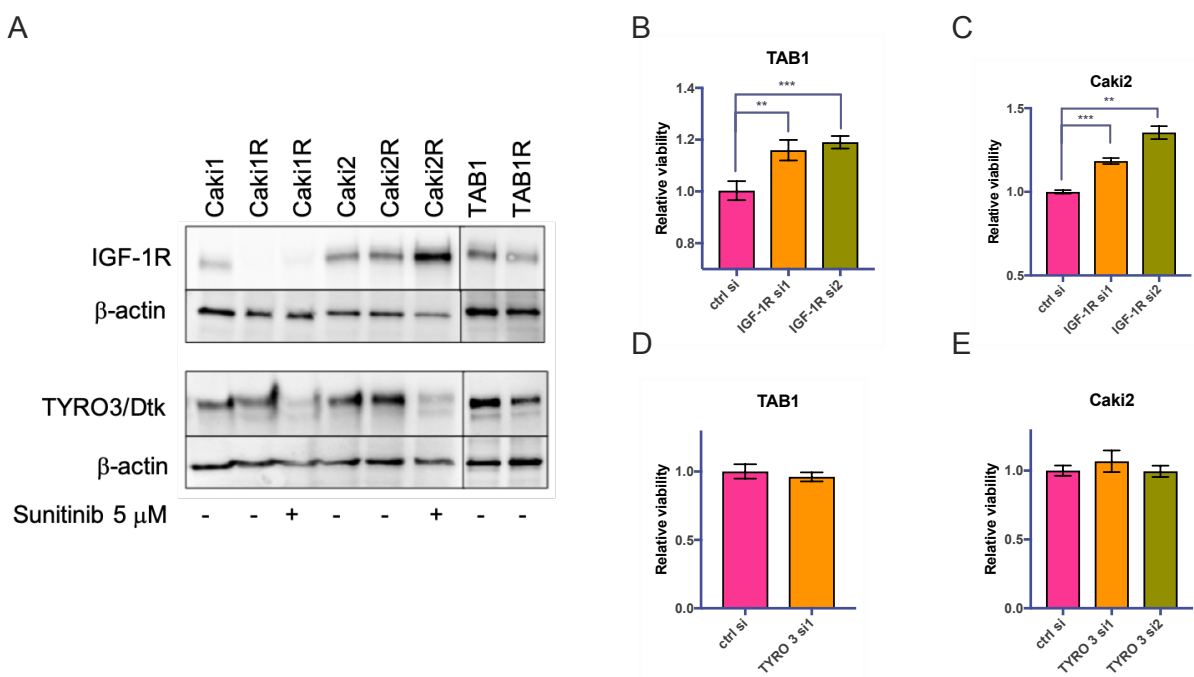
Figure 12: IGF-1R and TYRO3/Dtk protein regulation in sunitinib-resistant cell lines. IGF-1R protein expression in Caki1R, TAB1R and Caki2R next to parental cell lines (A, top). TYRO3/Dtk expression in resistant and native Caki and TAB1 cell lines (A, bottom). Transient knockdown with two different siRNAs against IGF-1R induced a significantly increased sunitinib resistance in TAB1 and Caki2 (B and C). The transient knockdown of TYRO3/Dtk siRNA in TAB1 and Caki2 did not show any effect on cell viability after 5 μM sunitinib treatment for 48 hours (n = 3) (D und E).

resistance to sunitinib in all knockdown cases in comparison to mock-transfected cells (Figure 12B and C). In contrast, siRNAs against TYRO3/Dtk had no effect on cell viability after sunitinib treatment in TAB1 and Caki2 (Figure 12D and E).

To further analyze the relevance of IGF-1R and TYRO3/Dtk for the (non-)response to sunitinib treatment, both genes were overexpressed in TAB1 and 1889c cells. In Caki cells, we were not able to sufficiently overexpress either gene (Figure 13A). Overexpression of IGF-1R in the resistant TAB1R and 1889c significantly sensitized
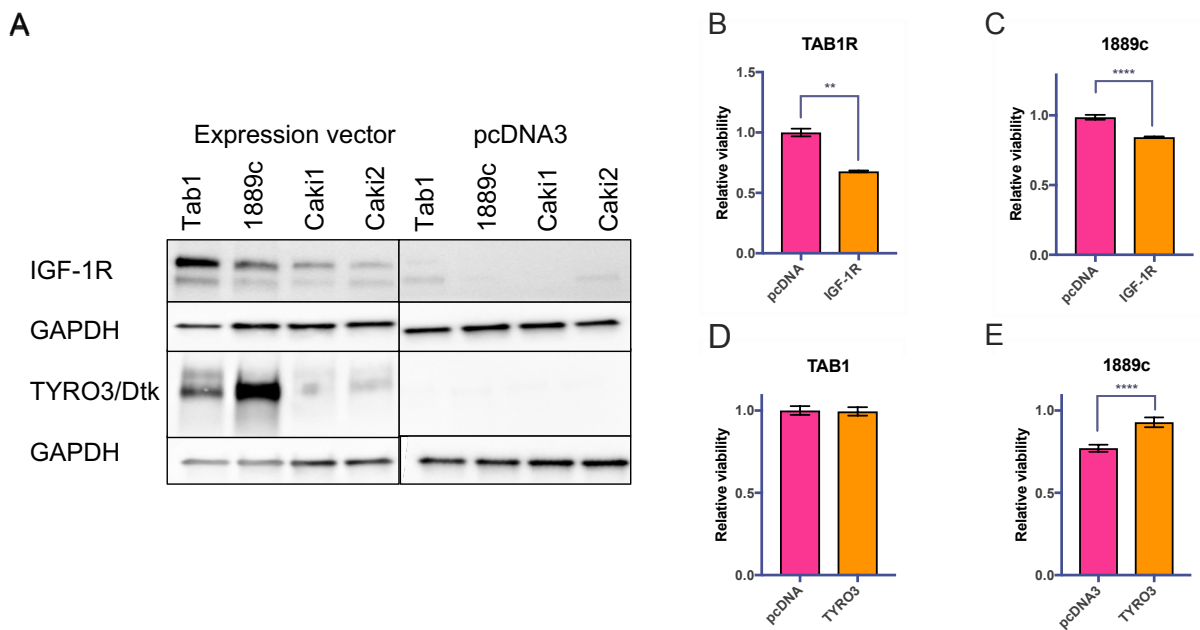
Figure 13: Overexpression of IGF-1R and TYRO3/Dtk in cell lines treated with sunitinib. The over expression of IGF-1R in the resistance-induced TAB1R and 1889c showed a reduced viability upon sunitinib treatment (C and D). Overexpression of TYRO3/Dtk showed no effect in TAB1 and significantly increased the resistance of 1889c after 48 hours of 5 μM sunitinib treatment (D and E). pcDNA was transfected as control vector.

both cell lines to sunitinib (5 μM over 48 h) (Figure13B and C). However, the overexpression of TYRO3/Dtk in the parental cell line TAB1 did not show any changes in the response to sunitinib, but it significantly decreased sunitinib sensitivity (Figure 13D and E).

3.13 pIGF1-R and TYRO3/Dtk do not correlate with SRI

We then sought to investigate the correlation between IGF-1R and TYRO3/Dtk and the corresponding SRI. Here, WB signals (Figure 14A) and phospho signals from the RTK arrays of IGF-1R and TYRO3/Dtk were compared to the specific SRI of the patient samples. Unfortunately, this did not result in any relevant correlation (Figure 14B – I).
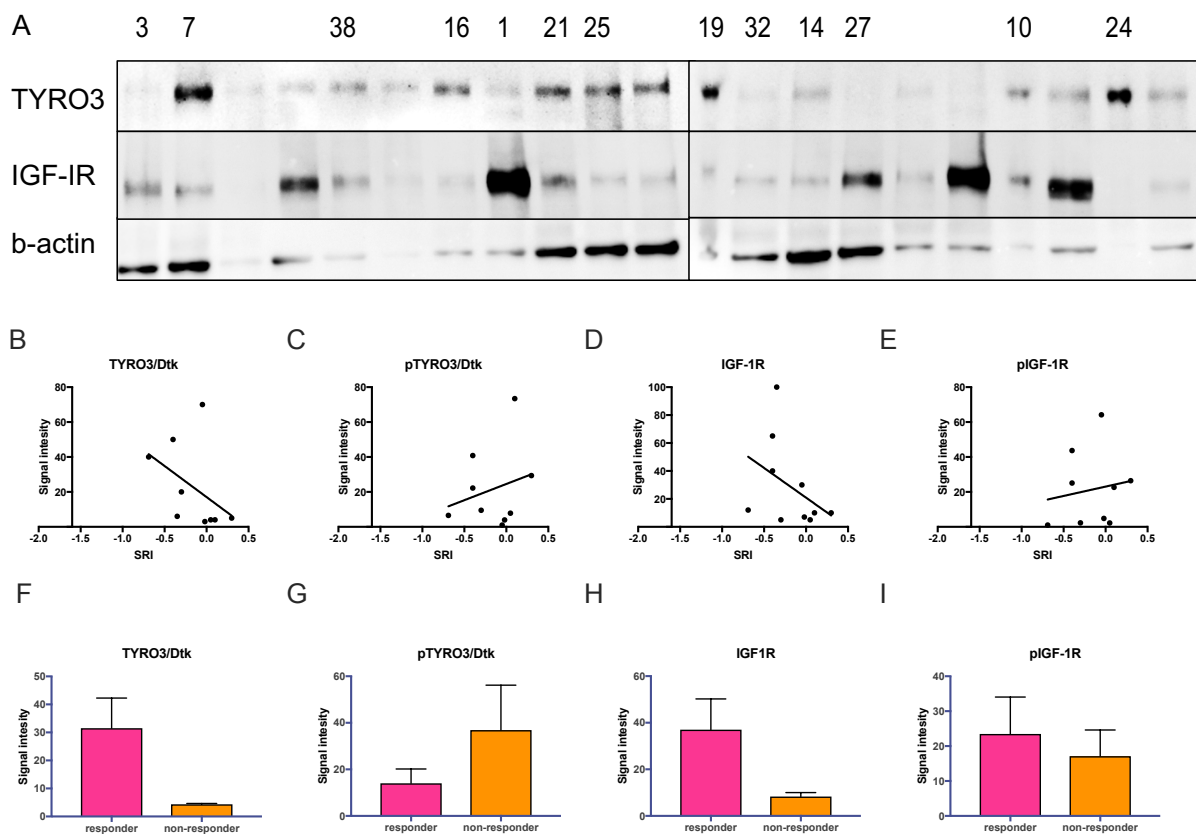
Figure 14: Correlation of IGF-1R and TYRO3/**Dtk with SRI.** WB of TYRO3/DTK and IGF-1R of 20 tissue lysates (A). WB signal intensities of TYRO3/Dtk (B) and IGF-1R (D) and of RTK phospho signals of TYRO3/Dtk (C) and IGF-1R (E) were correlated to the SRI of the specific sample. Comparison of the mean normalized WB signals (F and H) or the phospho signals (G and I) of the „responder" (negative SRI) against the "non-responder" (positive SRI). The correlations (B-E) and differences (F-I) did not reach the level of significance. WB numbering corresponds to Patient No.

There was a tendency towards an inverse correlation between IGF-1R and the SRI (R^2 = 0,2593, p<0.109) (Figure 14D) and the potential "responding" group showed increased IGF-1R levels in comparison to the "non-responder" group (Figure 14H). pTYRO3/Dtk even showed a tendency to a positive correlation to the SRI (Figure 14C and G).

DISCUSSION

Due to the rarity of TH and TC, very few randomized clinical trials for second-line therapies have been possible to date. The treatment options after total resection have thus long been limited to radiochemotherapy, but with high tumor recurrence rates. Recently, alternative second-line therapeutic options (such as kinase inhibitors) have been introduced largely on an empirical level (i.e. without a strong molecular rationale) [40], and the treatment choice is difficult since the available drugs are active only in a minority of patients with a particular histological tumor subtype. Predicting the response to therapeutic treatments such as sunitinib is a primary prerequisite of personalized medicine and would aid in the choice of treatment. In this study, we used RTK and MAPK phospho arrays to characterize the malignant TH and TC by their kinase activities and established a sunitinib response index (SRI) using a multi peptide array. We further focused on the functional analysis of predicted TYRO3/Dtk and IGF-1R as potential sunitinib targets and biomarkers for sunitinib response in malignant TH and TC.

RTK phospho arrays from 33 malignant TH and TC revealed EGFR as a highly activated kinase in over 70% of the cases. Recent studies in a limited number of patients suggested that EGFR antagonists such as cetuximab may provide effective treatment in specific cases [30-33]. However, the variable findings in these studies suggest that a more detailed approach is necessary to obtain better therapeutic results. Hierarchical cluster analyses of RTK phospho array analyses revealed two main dominant patterns, with either strong activation of EGFR alone or combined with strong activation of TYRO3/Dtk. Even though there was no connection of EGFR activation to clinical parameters, the significantly higher activation of TYRO3/Dtk in recurrent and metastatic tumors activity might be an indicator of disease progression of malignant TH and TC. This finding fit to data from several recent studies in which stronger TYRO3/Dtk phosphorylation was found to be associated with a worse prognosis in various cancer types[50, 51].

Hierarchical clustering of 14 MAPK arrays revealed three rather distinct groups within malignant TH and TC: p38δ and RSK1 were significantly differentially activated in a cluster-specific manner.

To adapt to environmental changes, cells activate p38MAPKs as one of the main signal transduction mechanisms. In mammals, there are four p38MAPK isoforms encoded by

different genes: p38α (MAPK14), p38β (MAPK 11), p38γ (MAPK 12), and p38δ (MAPK 13)[67]. Particularly p38α, the most studied p38MAPK, has been shown to play a role in innate immune responses and inflammation[67].The importance of p38γ and p38δ in cancers that are associated with chronic inflammation, also recently became evident[68]. In breast cancer, p38γ and p38δ in particular have been found to promote cancer progression, invasion and metastasis[69, 70]. Furthermore, a recent study in a p38γ and p38δ knock-out mouse model reported that activation of these specific MAPKs was important for early T cell development[71]. Furthermore, p38 has been linked to MG because it increases the expression of IL-6 and RANTES, which is likely to lead to pathological remodeling of the myasthenic thymus[72]. Therefore, p38MAPKs should be taken into consideration when studying thymic malignancies including TH and TC, MG, thymic inflammation in the elderly, and thymic involution.

RSK1 has been described in invasive melanoma[73] and has been proposed as a therapeutic target in triple negative breast carcinoma[74]. Therefore, it is possible that increased RSK1 activity could also indicate a more aggressive phenotype in malignant TH and TC.

In summary, the analysis of the RTK and MAPK phosphorylation arrays revealed TYRO3/Dtk as a potential prognostic marker in malignant TH and TC. The activities of p38MAPKs and RSK1 are increased in subgroups, but show no prognostic value. However, the specific activity of p38 MAPKs and the spectrum of their functions points to their potential use for following disease onset to metastasis in TH and TC.

For a more predictive clinical approach, we utilized kinase activity profiling as a potential tool for selecting sunitinib to treat malignant TH and TC. We established a sunitinib response index with the resistance-induced cell lines TAB1R and Caki2R in comparison to their native parental cells. To increase the discriminative power, and to stabilize the technical variances, we used the ratio of the measurement of each sample with and without sunitinib added during the assay. A similar approach has been published by Arni S. et al., who identified a potential predictive signature by characterizing 71 paired early-stage and non-neoplastic lung adenocarcinoma sample lysates in the presence or absence of the tyrosine kinase inhibitor gefitinib[57]. Applying the SRI to 8 cancer cell lines, we were able to validate the response in 5 cell lines. To increase the specificity of the SRI in the future, a bigger number of sunitinib resistance induced cell lines need to be included. Nevertheless, the application of the SRI to patient samples separated 17 malignant TH and TC into two well-defined groups: 7

potential sunitinib-resistant non-responders and 10 responders, including one long-term sunitinib-responding patient. A closer look at the potential non-responding group revealed 2 samples with a much higher index than the rest (Figure 10). Although these samples were not associated with any specific clinical features in the respective patients (who were not treated with sunitinib), it is possible that the observed massive *in vitro* resistance might predict sunitinib resistance *in vivo*. One observation we made was that the majority of the predicted resistant samples were TC, whereas on the responder side, there was only one known responder TC among the TH. This finding is in contrast to the observations described by Thomas et al.[39] in which TC patients had a higher frequency of response to sunitinib than TH. Further investigations are necessary to exclude technical biases or type-specific SRI separation.

The prediction of upstream kinases responsible for responsive and non-responsive phospho patterns identified TYRO3/Dtk as the main RTK and potential sunitinib target. This is in agreement with previously published data in patients who responded particularly well to sunitinib treatment, showing strong activation of certain RTKs, including TYRO3/Dtk [54]. A biologic activity of sunitinib on TYRO-3/Dtk has not been reported so far. TYRO3/Dtk and the other two known members of the TAM receptor family share a conserved sequence within the kinase domain and adhesion molecule-like extracellular domains, and are involved in many different cellular processes, including proliferation and survival, cell adhesion and migration. The TAM receptor family members are overexpressed in a variety of human cancers[8] and are suggested to be potentially oncogenic[51]. Moreover, TYRO3/Dtk has recently been described as a molecular target in bladder cancer. TYRO3/Dtk showed a higher expression than AXL and MERTK in muscle-invasive bladder cancer. Bladder tumor cells were sensitive to pan-TAM inhibitors, and TYRO3/Dtk depletion led to cell cycle inhibition and apoptosis[75]. Since TYRO3/Dtk also showed a significant association with disease progression (Figure 5), we wanted to validate its function with respect to the resistance against sunitinib.

In the course of a sunitinib resistance, development TYRO3/Dtk was downregulated in cell lines with induced resistance. Sunitinib treatment of resistant Caki2R and Caki1R almost abolished TYRO3/Dtk levels (Figure 12). Knockdown of TYRO3/Dtk did not have a remarkable effect the response to sunitinib, but its overexpression in 1889c made cells even more resistant to sunitinib treatment (Figure 13). In addition, we found that TYRO3/Dtk activity is also increased in progressive TH diseases. This proposes

that low activity of TYRO3/Dtk, independent of the protein level, is in addition to the SRI a potential predictive biomarker for the response of malignant TH and TC to sunitinib. These *in vitro* results are in contrast to observations in sunitinib responding patients and point out that TYRO3/Dtk alone is not sufficient to predict treatment response. Therefore, determination of TYRO3/Dtk kinase activity warrants evaluation as a predictive biomarker in prospective clinical trials. Although IGF-1R does not seem to have the predictive potential upstream kinase in the current setting, sunitinib has previously been shown to be active against IGF-1R[26]. Furthermore, strong activity of IGF-1R in ex vivo biopsies was previously observed in sunitinib-responsive TC patients[38].

The knockdown of IGF-1R in the native cell lines TAB1 and Caki2 showed a significant decrease in response to sunitinib. The overexpression led to an increased response to sunitinib in resistant TAB1R as well as in the TC cell line 1889c. This strongly suggests that IGF-1R is involved in the response to sunitinib, and that activation of IGF-1R is an indicator for treatment response (Figure 14).

There are several possible explanations for why we could not show a clear correlation between expression and activation of IGF-1R and TYRO3/Dtk with the established SRI. The rather small group size is most likely one of the major factors. Analysis of RTK and MAPK arrays revealed a large heterogeneity of kinase activity among the samples even in the distinct group of malignant TH and TC. An accurate and standardized treatment after resection is of importance for future studies to avoid degradation bias.

In summary, in this study, we characterized malignant TH and TC using RTK and MAPK activity arrays. This revealed a large heterogeneity of kinase activities, particularly concerning EGFR, TYRO3/Dtk and members of the p38 MAPK family that were strongly activated in specific subgroups. p38 MAPKs are of specific interest, since p38δ isoforms might help us understand the origin of the tumor development in connection with chronic inflammation. Furthermore, we present a novel, experimentally partially validated predictor of sunitinib response in 8 cell lines of malignant TH and TC that is based on RTK activity assay. We also validated IGF1-R and TYRO3/Dtk as potential biomarkers and possible sunitinib-resistance indicators. Future clinical trials should include IGF1R and TYRO3/Dtk for validation of the SRI.

4   SUMMARY

Metastatic and recurrent malignant thymomas (TH) and thymic carcinomas (TC) are generally refractory to current empiric radiochemotherapies, thus warranting the search for novel second-line therapeutic strategies. The multi-target tyrosine kinase inhibitor sunitinib has been shown to induce partial remissions and to prolong overall survival of patients with aggressive TH and TC. However, although sunitinib has been proposed as an alternative treatment option in refractory disease, treatment response is only partial, and not all patients benefit equally. For a more accurate response prediction, new biomarkers are needed.

In this study, we used phospho receptor tyrosine kinase (RTK) and MAPK arrays as well as a multiplex tyrosine phosphorylation assay containing 144 kinase substrates to characterize malignant TH and TC and to generate a sunitinib response index (SRI) using sunitinib resistance-induced cell lines. The RTK and MAPK arrays stratified the patients into two main dominant phosphor patterns: Pattern 1 was characterized by a strong activation of EGFR while pattern 2 was typified by a strong activation of TYRO3/Dtk. This activation of TYRO3/Dtk correlated with recurrence and metastatic spread of malignant TH. p38δ and RSK1 were cluster-specifically activated in the MAPKs but showed no specific disease correlation. The SRI was functionally validated in several cell lines, and the application of the SRI to native malignant TH and TC samples identified a potentially sunitinib-responsive and a potentially sunitinib-resistant group. Among the predicted upstream kinases, TYRO3/Dtk belonged to the top candidates responsible for sunitinib response. TYRO3/Dtk and the highly activated IGF-1R in responsive patients were also functionally validated. Specific siRNA knockdowns in sunitinib-resistant cell lines and overexpression confirmed the functional relevance of TYRO3/Dtk and IGF1-R for sunitinib resistance.

We present the SRI as a new approach to the resistance prediction of sunitinib in malignant TH and TC and propose that the activity level of TYRO3/Dtk and IGF-1R could serve as markers to aid in treatment decisions. The results of this in vitro investigation need validation of the SRI in prospective clinical trials.

5 REFERENCES

1. Hollander, GA, Wang, B, Nichogiannopoulou, A, Platenburg, PP, van Ewijk, W, Burakoff, SJ, Gutierrez-Ramos, JC, Terhorst, C: Developmental control point in induction of thymic cortex regulated by a subpopulation of prothymocytes. *Nature,* 373**:** 350-353, 1995.

2. van Ewijk, W, Hollander, G, Terhorst, C, Wang, B: Stepwise development of thymic microenvironments in vivo is regulated by thymocyte subsets. *Development,* 127**:** 1583-1591, 2000.

3. Patel, DD, Whichard, LP, Radcliff, G, Denning, SM, Haynes, BF: Characterization of human thymic epithelial cell surface antigens: phenotypic similarity of thymic epithelial cells to epidermal keratinocytes. *J Clin Immunol,* 15**:** 80-92, 1995.

4. Boehm, T, Bleul, CC: The evolutionary history of lymphoid organs. *Nat Immunol,* 8**:** 131-135, 2007.

5. Ströbel, P, Marx, A: Thymus. In: *H K Müller-Hermelink, H H Kreipe (Hrsg), Pathologie – Knochenmark, Lymphatisches System, Milz, Thymus,.* Springer-Verlag GmbH Deutschland 2018, 2018.

6. Steinmann, GG, Klaus, B, Muller-Hermelink, HK: The involution of the ageing human thymic epithelium is independent of puberty. A morphometric study. *Scand J Immunol,* 22**:** 563-575, 1985.

7. Song, Y, Su, M, Panchatsharam, P, Rood, D, Lai, L: c-Met signalling is required for efficient postnatal thymic regeneration and repair. *Immunology,* 144**:** 245-253, 2015.

8. Gregersen, PK, Kosoy, R, Lee, AT, Lamb, J, Sussman, J, McKee, D, Simpfendorfer, KR, Pirskanen-Matell, R, Piehl, F, Pan-Hammarstrom, Q, Verschuuren, JJ, Titulaer, MJ, Niks, EH, Marx, A, Strobel, P, Tackenberg, B, Putz, M, Maniaol, A, Elsais, A, Tallaksen, C, Harbo, HF, Lie, BA, Raychaudhuri, S, de Bakker, PI, Melms, A, Garchon, HJ, Willcox, N, Hammarstrom, L, Seldin, MF: Risk for myasthenia gravis maps to a (151) Pro-->Ala change in TNIP1 and to human leukocyte antigen-B*08. *Ann Neurol,* 72**:** 927-935, 2012.

9. Lefvert, AK, Zhao, Y, Ramanujam, R, Yu, S, Pirskanen, R, Hammarstrom, L: PTPN22 R620W promotes production of anti-AChR autoantibodies and IL-2 in myasthenia gravis. *J Neuroimmunol,* 197**:** 110-113, 2008.

10. Macchiarini, P, Ostertag, H: Uncommon primary mediastinal tumours. *Lancet Oncol,* 5**:** 107-118, 2004.

11. Marx, A, Chan, JK, Coindre, JM, Detterbeck, F, Girard, N, Harris, NL, Jaffe, ES, Kurrer, MO, Marom, EM, Moreira, AL, Mukai, K, Orazi, A, Strobel, P: The 2015 World Health Organization Classification of Tumors of the Thymus: Continuity and Changes. *J Thorac Oncol,* 10**:** 1383-1395, 2015.

12. P. Ströbel, AM: Thymus. In: *Pathologie: Knochenmark, Lymphatisches System, Milz, Thymus.* Hans Konrad Müller-HermelinkHans H. Kreipe, 2018.

13. Weis, CA, Yao, X, Deng, Y, Detterbeck, FC, Marino, M, Nicholson, AG, Huang, J, Strobel, P, Antonicelli, A, Marx, A, Contributors to the, IRD: The impact of thymoma histotype on prognosis in a worldwide database. *J Thorac Oncol,* 10**:** 367-372, 2015.

14. P. Ströbel, AM: Thymus. In: *Pathologie – Knochenmark, Lymphatisches System, Milz, Thymus,.* edited by H. K. MÜLLER-HERMELINK, H. H. K., © Springer-Verlag GmbH Deutschland 2018, 2018.

15. Aaby, P, Marx, C, Trautner, S, Rudaa, D, Hasselbalch, H, Jensen, H, Lisse, I: Thymus size at birth is associated with infant mortality: a community study from Guinea-Bissau. *Acta Paediatr,* 91**:** 698-703, 2002.

16. Detterbeck, FC, Stratton, K, Giroux, D, Asamura, H, Crowley, J, Falkson, C, Filosso, PL, Frazier, AA, Giaccone, G, Huang, J, Kim, J, Kondo, K, Lucchi, M, Marino, M, Marom, EM, Nicholson, AG, Okumura, M, Ruffini, E, Van Schil, P, Staging, Prognostic Factors, C, Members of the Advisory, B, Participating Institutions of the Thymic, D: The IASLC/ITMIG Thymic Epithelial Tumors Staging Project: proposal for an evidence-based stage classification system for the forthcoming (8th) edition of the TNM classification of malignant tumors. *J Thorac Oncol,* 9**:** S65-72, 2014.
17. Gomez, D, Komaki, R, Yu, J, Ikushima, H, Bezjak, A: Radiation therapy definitions and reporting guidelines for thymic malignancies. *J Thorac Oncol,* 6**:** S1743-1748, 2011.
18. Kondo, K, Monden, Y: Lymphogenous and hematogenous metastasis of thymic epithelial tumors. *Ann Thorac Surg,* 76**:** 1859-1864; discussion 1864-1855, 2003.
19. Ahmad, U, Yao, X, Detterbeck, F, Huang, J, Antonicelli, A, Filosso, PL, Ruffini, E, Travis, W, Jones, DR, Zhan, Y, Lucchi, M, Rimner, A: Thymic carcinoma outcomes and prognosis: results of an international analysis. *J Thorac Cardiovasc Surg,* 149**:** 95-100, 101 e101-102, 2015.
20. Huang, J, Rizk, NP, Travis, WD, Riely, GJ, Park, BJ, Bains, MS, Dycoco, J, Flores, RM, Downey, RJ, Rusch, VW: Comparison of patterns of relapse in thymic carcinoma and thymoma. *J Thorac Cardiovasc Surg,* 138**:** 26-31, 2009.
21. Travis, WD, Brambilla, E, Burke, AP, Marx, A, Nicholson, AG: Introduction to The 2015 World Health Organization Classification of Tumors of the Lung, Pleura, Thymus, and Heart. *J Thorac Oncol,* 10**:** 1240-1242, 2015.
22. Radovich, M, Pickering, CR, Felau, I, Ha, G, Zhang, H, Jo, H, Hoadley, KA, Anur, P, Zhang, J, McLellan, M, Bowlby, R, Matthew, T, Danilova, L, Hegde, AM, Kim, J, Leiserson, MDM, Sethi, G, Lu, C, Ryan, M, Su, X, Cherniack, AD, Robertson, G, Akbani, R, Spellman, P, Weinstein, JN, Hayes, DN, Raphael, B, Lichtenberg, T, Leraas, K, Zenklusen, JC, Cancer Genome Atlas, N, Fujimoto, J, Scapulatempo-Neto, C, Moreira, AL, Hwang, D, Huang, J, Marino, M, Korst, R, Giaccone, G, Gokmen-Polar, Y, Badve, S, Rajan, A, Strobel, P, Girard, N, Tsao, MS, Marx, A, Tsao, AS, Loehrer, PJ: The Integrated Genomic Landscape of Thymic Epithelial Tumors. *Cancer Cell,* 33**:** 244-258 e210, 2018.
23. Lee, GY, Yang, WI, Jeung, HC, Kim, SC, Seo, MY, Park, CH, Chung, HC, Rha, SY: Genome-wide genetic aberrations of thymoma using cDNA microarray based comparative genomic hybridization. *BMC Genomics,* 8**:** 305, 2007.
24. Girard, N, Shen, R, Guo, T, Zakowski, MF, Heguy, A, Riely, GJ, Huang, J, Lau, C, Lash, AE, Ladanyi, M, Viale, A, Antonescu, CR, Travis, WD, Rusch, VW, Kris, MG, Pao, W: Comprehensive genomic analysis reveals clinically relevant molecular distinctions between thymic carcinomas and thymomas. *Clin Cancer Res,* 15**:** 6790-6799, 2009.
25. Petrini, I, Meltzer, PS, Zucali, PA, Luo, J, Lee, C, Santoro, A, Lee, HS, Killian, KJ, Wang, Y, Tsokos, M, Roncalli, M, Steinberg, SM, Wang, Y, Giaccone, G: Copy number aberrations of BCL2 and CDKN2A/B identified by array-CGH in thymic epithelial tumors. *Cell Death Dis,* 3**:** e351, 2012.
26. Tateyama, H, Eimoto, T, Tada, T, Mizuno, T, Inagaki, H, Hata, A, Sasaki, M, Masaoka, A: p53 protein expression and p53 gene mutation in thymic epithelial tumors. An immunohistochemical and DNA sequencing study. *Am J Clin Pathol,* 104**:** 375-381, 1995.
27. Wang, Y, Thomas, A, Lau, C, Rajan, A, Zhu, Y, Killian, JK, Petrini, I, Pham, T, Morrow, B, Zhong, X, Meltzer, PS, Giaccone, G: Mutations of epigenetic regulatory genes are common in thymic carcinomas. *Sci Rep,* 4**:** 7336, 2014.
28. Strobel, P, Hartmann, M, Jakob, A, Mikesch, K, Brink, I, Dirnhofer, S, Marx, A: Thymic carcinoma with overexpression of mutated KIT and the response to imatinib. *N Engl J Med,* 350**:** 2625-2626, 2004.

29. Ried, M: Therapie von Thymomen und Thymuskarzinomen. *best practice onkologie,* 12**:** 206-214, 2017.

30. Strobel, P, Knop, S, Einsele, H, Muller-Hermelink, HK, Marx, A: [Therapy-relevant mutations of receptor tyrosine kinases in malignant thymomas and thymic carcinomas: a therapeutic perspective]. *Verh Dtsch Ges Pathol,* 91**:** 177-186, 2007.

31. Christodoulou, C, Murray, S, Dahabreh, J, Petraki, K, Nikolakopoulou, A, Mavri, A, Skarlos, D: Response of malignant thymoma to erlotinib. *Ann Oncol,* 19**:** 1361-1362, 2008.

32. Palmieri, G, Marino, M, Salvatore, M, Budillon, A, Meo, G, Caraglia, M, Montella, L: Cetuximab is an active treatment of metastatic and chemorefractory thymoma. *Front Biosci,* 12**:** 757-761, 2007.

33. Farina, G, Garassino, MC, Gambacorta, M, La Verde, N, Gherardi, G, Scanni, A: Response of thymoma to cetuximab. *Lancet Oncol,* 8**:** 449-450, 2007.

34. Girard, N: Targeted therapies for thymic malignancies. *Thorac Surg Clin,* 21**:** 115-123, viii, 2011.

35. Le Tourneau, C, Raymond, E, Faivre, S: Sunitinib: a novel tyrosine kinase inhibitor. A brief review of its therapeutic potential in the treatment of renal carcinoma and gastrointestinal stromal tumors (GIST). *Ther Clin Risk Manag,* 3**:** 341-348, 2007.

36. Burstein, HJ, Elias, AD, Rugo, HS, Cobleigh, MA, Wolff, AC, Eisenberg, PD, Lehman, M, Adams, BJ, Bello, CL, DePrimo, SE, Baum, CM, Miller, KD: Phase II study of sunitinib malate, an oral multitargeted tyrosine kinase inhibitor, in patients with metastatic breast cancer previously treated with an anthracycline and a taxane. *J Clin Oncol,* 26**:** 1810-1816, 2008.

37. Faivre, S, Demetri, G, Sargent, W, Raymond, E: Molecular basis for sunitinib efficacy and future clinical development. *Nat Rev Drug Discov,* 6**:** 734-745, 2007.

38. Strobel, P, Bargou, R, Wolff, A, Spitzer, D, Manegold, C, Dimitrakopoulou-Strauss, A, Strauss, L, Sauer, C, Mayer, F, Hohenberger, P, Marx, A: Sunitinib in metastatic thymic carcinomas: laboratory findings and initial clinical experience. *Br J Cancer,* 103**:** 196-200, 2010.

39. Thomas, A, Rajan, A, Berman, A, Tomita, Y, Brzezniak, C, Lee, MJ, Lee, S, Ling, A, Spittler, AJ, Carter, CA, Guha, U, Wang, Y, Szabo, E, Meltzer, P, Steinberg, SM, Trepel, JB, Loehrer, PJ, Giaccone, G: Sunitinib in patients with chemotherapy-refractory thymoma and thymic carcinoma: an open-label phase 2 trial. *Lancet Oncol,* 16**:** 177-186, 2015.

40. Marx, A, Weis, CA: Sunitinib in thymic carcinoma: enigmas still unresolved. *Lancet Oncol,* 16**:** 124-125, 2015.

41. Folkvord, S, Flatmark, K, Dueland, S, de Wijn, R, Groholt, KK, Hole, KH, Nesland, JM, Ruijtenbeek, R, Boender, PJ, Johansen, M, Giercksky, KE, Ree, AH: Prediction of response to preoperative chemoradiotherapy in rectal cancer by multiplex kinase activity profiling. *Int J Radiat Oncol Biol Phys,* 78**:** 555-562, 2010.

42. Versele, M, Talloen, W, Rockx, C, Geerts, T, Janssen, B, Lavrijssen, T, King, P, Gohlmann, HW, Page, M, Perera, T: Response prediction to a multitargeted kinase inhibitor in cancer cell lines and xenograft tumors using high-content tyrosine peptide arrays with a kinetic readout. *Mol Cancer Ther,* 8**:** 1846-1855, 2009.

43. Gotink, KJ, Rovithi, M, de Haas, RR, Honeywell, RJ, Dekker, H, Poel, D, Azijli, K, Peters, GJ, Broxterman, HJ, Verheul, HM: Cross-resistance to clinically used tyrosine kinase inhibitors sunitinib, sorafenib and pazopanib. *Cell Oncol (Dordr),* 38**:** 119-129, 2015.

44. Saelen, MG, Flatmark, K, Folkvord, S, de Wijn, R, Rasmussen, H, Fodstad, O, Ree, AH: Tumor kinase activity in locally advanced rectal cancer: angiogenic signaling and early systemic dissemination. *Angiogenesis,* 14**:** 481-489, 2011.

45. Sikkema, AH, Diks, SH, den Dunnen, WF, ter Elst, A, Scherpen, FJ, Hoving, EW, Ruijtenbeek, R, Boender, PJ, de Wijn, R, Kamps, WA, Peppelenbosch, MP, de Bont, ES: Kinome profiling in pediatric brain tumors as a new approach for target discovery. *Cancer Res,* 69**:** 5987-5995, 2009.

46. Ter Elst, A, Diks, SH, Kampen, KR, Hoogerbrugge, PM, Ruijtenbeek, R, Boender, PJ, Sikkema, AH, Scherpen, FJ, Kamps, WA, Peppelenbosch, MP, de Bont, ES: Identification of new possible targets for leukemia treatment by kinase activity profiling. *Leuk Lymphoma,* 52**:** 122-130, 2011.

47. Massague, J, Czech, MP: The subunit structures of two distinct receptors for insulin-like growth factors I and II and their relationship to the insulin receptor. *J Biol Chem,* 257**:** 5038-5045, 1982.

48. Li, R, Pourpak, A, Morris, SW: Inhibition of the insulin-like growth factor-1 receptor (IGF1R) tyrosine kinase as a novel cancer therapy approach. *J Med Chem,* 52**:** 4981-5004, 2009.

49. Lu, Q, Gore, M, Zhang, Q, Camenisch, T, Boast, S, Casagranda, F, Lai, C, Skinner, MK, Klein, R, Matsushima, GK, Earp, HS, Goff, SP, Lemke, G: Tyro-3 family receptors are essential regulators of mammalian spermatogenesis. *Nature,* 398**:** 723-728, 1999.

50. Smart, SK, Vasileiadi, E, Wang, X, DeRyckere, D, Graham, DK: The Emerging Role of TYRO3 as a Therapeutic Target in Cancer. *Cancers (Basel),* 10, 2018.

51. Hsu, PL, Jou, J, Tsai, SJ: TYRO3: A potential therapeutic target in cancer. *Exp Biol Med (Maywood),* 244**:** 83-99, 2019.

52. Vouri, M, Hafizi, S: TAM Receptor Tyrosine Kinases in Cancer Drug Resistance. *Cancer Res,* 77**:** 2775-2778, 2017.

53. Schmitz, R, Valls, AF, Yerbes, R, von Richter, S, Kahlert, C, Loges, S, Weitz, J, Schneider, M, Ruiz de Almodovar, C, Ulrich, A, Schmidt, T: TAM receptors Tyro3 and Mer as novel targets in colorectal cancer. *Oncotarget,* 7**:** 56355-56370, 2016.

54. Strobel, P, Hohenberger, P, Marx, A: Thymoma and thymic carcinoma: molecular pathology and targeted therapy. *J Thorac Oncol,* 5**:** S286-290, 2010.

55. Gokmen-Polar, Y, Sanders, KL, Goswami, CP, Cano, OD, Zaheer, NA, Jain, RK, Kesler, KA, Nelson, RP, Jr., Vance, GH, Smith, D, Li, L, Cardoso, AA, Badve, S, Loehrer, PJ, Sr., Sledge, GW, Jr.: Establishment and characterization of a novel cell line derived from human thymoma AB tumor. *Lab Invest,* 92**:** 1564-1573, 2012.

56. Masaoka, A, Monden, Y, Nakahara, K, Tanioka, T: Follow-up study of thymomas with special reference to their clinical stages. *Cancer,* 48**:** 2485-2492, 1981.

57. Arni, S, Le, THN, de Wijn, R, Garcia-Villegas, R, Dankers, M, Weder, W, Hillinger, S: Ex vivo multiplex profiling of protein tyrosine kinase activities in early stages of human lung adenocarcinoma. *Oncotarget,* 8**:** 68599-68613, 2017.

58. Maretto, I, Pomerri, F, Pucciarelli, S, Mescoli, C, Belluco, E, Burzi, S, Rugge, M, Muzzio, PC, Nitti, D: The potential of restaging in the prediction of pathologic response after preoperative chemoradiotherapy for rectal cancer. *Ann Surg Oncol,* 14**:** 455-461, 2007.

59. Tahiri, A, Roe, K, Ree, AH, de Wijn, R, Risberg, K, Busch, C, Lonning, PE, Kristensen, V, Geisler, J: Differential inhibition of ex-vivo tumor kinase activity by vemurafenib in BRAF(V600E) and BRAF wild-type metastatic malignant melanoma. *PLoS One,* 8**:** e72692, 2013.

60. Andersen, AH, Rayens, WS, Liu, Y, Smith, CD: Partial least squares for discrimination in fMRI data. *Magn Reson Imaging,* 30**:** 446-452, 2012.

61. Girard, N, Teruya-Feldstein, J, Payabyab, EC, Riely, GJ, Rusch, VW, Kris, MG, Zakowski, MF: Insulin-like growth factor-1 receptor expression in thymic malignancies. *J Thorac Oncol,* 5**:** 1439-1446, 2010.

62. Rajan, A, Carter, CA, Berman, A, Cao, L, Kelly, RJ, Thomas, A, Khozin, S, Chavez, AL, Bergagnini, I, Scepura, B, Szabo, E, Lee, MJ, Trepel, JB, Browne, SK, Rosen, LB, Yu,

Y, Steinberg, SM, Chen, HX, Riely, GJ, Giaccone, G: Cixutumumab for patients with recurrent or refractory advanced thymic epithelial tumours: a multicentre, open-label, phase 2 trial. *Lancet Oncol,* 15**:** 191-200, 2014.

63. Topcul, MR, Cetin, I: In vitro cytotoxic effect of tyrosine kinase inhibitor sunitinib malate alone and in combination with hyperthermia on breast adenocarcinoma MCF-7 cells. *J BUON,* 21**:** 556-563, 2016.

64. Shin, HW, Cho, CH, Kim, TY, Park, JW: Sunitinib deregulates tumor adaptation to hypoxia by inhibiting HIF-1alpha synthesis in HT-29 colon cancer cells. *Biochem Biophys Res Commun,* 398**:** 205-211, 2010.

65. Sun, J, Sun, Q, Brown, MF, Dudgeon, C, Chandler, J, Xu, X, Shu, Y, Zhang, L, Yu, J: The multi-targeted kinase inhibitor sunitinib induces apoptosis in colon cancer cells via PUMA. *PLoS One,* 7**:** e43158, 2012.

66. Oudard, S, Geoffrois, L, Guillot, A, Chevreau, C, Deville, JL, Falkowski, S, Boyle, H, Baciuchka, M, Gimel, P, Laguerre, B, Laramas, M, Pfister, C, Topart, D, Rolland, F, Legouffe, E, Denechere, G, Amela, EY, Abadie-Lacourtoisie, S, Gross-Goupil, M: Clinical activity of sunitinib rechallenge in metastatic renal cell carcinoma-Results of the REchallenge with SUnitinib in MEtastatic RCC (RESUME) Study. *Eur J Cancer,* 62**:** 28-35, 2016.

67. Cuenda, A, Rousseau, S: p38 MAP-kinases pathway regulation, function and role in human diseases. *Biochim Biophys Acta,* 1773**:** 1358-1375, 2007.

68. Escos, A, Risco, A, Alsina-Beauchamp, D, Cuenda, A: p38gamma and p38delta Mitogen Activated Protein Kinases (MAPKs), New Stars in the MAPK Galaxy. *Front Cell Dev Biol,* 4**:** 31, 2016.

69. Wada, M, Canals, D, Adada, M, Coant, N, Salama, MF, Helke, KL, Arthur, JS, Shroyer, KR, Kitatani, K, Obeid, LM, Hannun, YA: P38 delta MAPK promotes breast cancer progression and lung metastasis by enhancing cell proliferation and cell detachment. *Oncogene,* 36**:** 6649-6657, 2017.

70. Koul, HK, Pal, M, Koul, S: Role of p38 MAP Kinase Signal Transduction in Solid Tumors. *Genes Cancer,* 4**:** 342-359, 2013.

71. Risco, A, Martin-Serrano, MA, Barber, DF, Cuenda, A: p38gamma and p38delta Are Involved in T Lymphocyte Development. *Front Immunol,* 9**:** 65, 2018.

72. Colombara, M, Antonini, V, Riviera, AP, Mainiero, F, Strippoli, R, Merola, M, Fracasso, G, Poffe, O, Brutti, N, Tridente, G, Colombatti, M, Ramarli, D: Constitutive activation of p38 and ERK1/2 MAPKs in epithelial cells of myasthenic thymus leads to IL-6 and RANTES overexpression: effects on survival and migration of peripheral T and B cells. *J Immunol,* 175**:** 7021-7028, 2005.

73. Salhi, A, Farhadian, JA, Giles, KM, Vega-Saenz de Miera, E, Silva, IP, Bourque, C, Yeh, K, Chhangawala, S, Wang, J, Ye, F, Zhang, DY, Hernando-Monge, E, Houvras, Y, Osman, I: RSK1 activation promotes invasion in nodular melanoma. *Am J Pathol,* 185**:** 704-716, 2015.

74. Ludwik, KA, Campbell, JP, Li, M, Li, Y, Sandusky, ZM, Pasic, L, Sowder, ME, Brenin, DR, Pietenpol, JA, O'Doherty, GA, Lannigan, DA: Development of a RSK Inhibitor as a Novel Therapy for Triple-Negative Breast Cancer. *Mol Cancer Ther,* 15**:** 2598-2608, 2016.

75. Dufour, F, Silina, L, Neyret-Kahn, H, Moreno-Vega, A, Krucker, C, Karboul, N, Dorland-Galliot, M, Maille, P, Chapeaublanc, E, Allory, Y, Stransky, N, Haegel, H, Menguy, T, Duong, V, Radvanyi, F, Bernard-Pierrot, I: TYRO3 as a molecular target for growth inhibition and apoptosis induction in bladder cancer. *Br J Cancer,* 120**:** 555-564, 2019.

6 SUPPLEMENTAL MATERIALS

Supplemental Table 1: Normalized phospho signal values of RTK arrays. Mean signals of double spots were normalized to positive controls after background correction. Negative and 0 values were set to 1. Patient Nr. Correspond to Patient sample list (see Tab13)

Patient Nr.	EphA3	EphA2	Flt-3	FGF R4	ROR2	MuSK	SCF R	EphB1	HGF R	VEGF R3	FGF R3	EphA6	EphB4	EphA4	FGF R1	TrkB	PDGF R alpha	VEGF R1
2	5,11	3,44	1,00	5,36	10,16	0,13	1,00	1,00	33,39	1,00	3,53	10,21	1,00	11,16	2,78	4,79	2,85	1,00
3	1,55	0,29	1,00	1,00	1,91	1,00	5,45	1,40	2,28	1,00	1,00	8,39	1,43	3,07	1,00	0,72	0,00	1,00
4	1,00	1,00	1,00	1,00	2,32	1,00	2,70	2,12	0,27	10,36	15,51	1,00	12,57	6,67	1,00	1,40	1,00	9,47
5	1,00	1,00	1,11	1,00	1,00	1,00	2,12	3,92	1,41	3,56	5,56	6,44	2,62	1,00	1,00	3,51	2,60	2,23
6	2,61	4,26	9,75	6,80	7,34	7,34	6,76	7,19	4,96	9,76	7,08	19,27	5,50	9,91	2,19	7,37	5,30	7,16
7	1,00	1,00	7,34	3,16	3,22	1,39	6,13	2,75	5,54	7,12	8,36	13,42	2,20	1,92	7,29	2,65	4,72	2,59
8	1,00	1,00	1,51	1,00	1,73	1,00	2,94	2,43	4,30	4,66	1,00	59,98	1,00	1,00	8,05	5,47	2,55	1,00
9	3,16	20,31	15,59	6,09	71,45	22,60	7,36	9,70	1,00	33,43	2,34	24,43	8,76	6,87	2,11	7,88	5,17	8,54
10	1,00	1,00	1,00	1,00	3,82	1,00	1,00	2,01	0,31	3,19	1,00	4,57	3,08	0,57	0,19	3,15	0,76	1,23
11	1,00	1,00	109,11	47,37	1,00	68,68	126,55	82,78	58,05	124,03	82,12	67,52	90,80	1,00	105,32	94,47	113,63	104,53
12	1,00	1,00	1,00	1,00	1,00	1,00	1,00	5,09	1,00	1,00	1,00	1,00	1,00	37,14	1,00	1,00	1,00	1,00
13	1,00	1,00	1,00	1,00	1,00	1,00	17,09	18,81	1,00	1,00	1,00	31,71	1,00	1,00	19,03	1,00	5,77	1,00
14	0,25	0,98	2,88	2,54	2,96	2,47	5,68	6,03	9,03	3,35	5,98	11,86	3,62	1,10	7,11	7,07	5,91	3,75
15	8,80	8,37	15,04	23,50	26,98	17,97	17,14	18,68	21,53	23,38	50,16	26,48	15,18	21,57	21,82	22,94	19,44	10,79
16	1,00	1,00	1,00	1,00	4,12	1,00	1,00	1,00	1,00	1,00	3,07	1,00	1,00	1,00	1,00	1,00	1,00	1,00
17	1,00	1,00	3,20	1,45	1,00	2,28	3,00	6,62	1,81	4,22	7,14	14,70	3,78	1,00	1,62	6,11	4,04	3,18
18	1,00	1,00	1,00	1,00	1,00	1,00	1,00	1,00	1,00	1,00	13,72	0,04	1,00	1,00	1,00	1,00	11,00	1,00
19	1,00	1,00	1,00	1,00	1,00	1,00	175,00	1,00	20,05	1,00	50,42	12,49	1,00	1,35	1,00	1,00	4,45	42,12
20	1,00	1,00	1,00	1,00	1,00	1,00	1,00	1,00	1,00	1,00	1,00	1,00	1,00	1,00	1,00	1,00	1,00	1,00
21	1,00	1,00	1,00	1,00	1,00	1,00	1,00	1,00	1,00	1,00	1,00	1,00	1,00	1,00	1,00	1,00	1,00	1,00
24	6,57	6,31	1,00	1,00	11,64	7,72	1,00	1,00	1,00	9,87	10,25	1,00	1,00	1,00	1,00	1,00	1,00	1,00
26	27,62	72,17	48,66	17,12	1,00	35,28	0,37	1,00	1,00	45,80	35,81	1,00	1,73	51,19	15,93	1,00	81,91	0,63
27	0,62	5,40	4,58	6,76	3,01	15,60	1,00	1,00	1,00	12,13	3,78	1,00	1,00	4,37	1,00	1,00	1,00	1,00
28	7,86	2,24	11,68	5,64	17,10	9,06	11,04	22,57	20,50	20,99	15,42	50,00	7,83	0,40	5,86	22,60	12,04	14,44
29	1,00	3,59	8,04	3,37	4,79	8,37	38,59	1,00	3,62	13,78	11,99	1,00	11,15	2,93	8,67	0,60	5,88	10,80
31	1,00	1,00	1,00	1,00	1,00	1,00	1,00	1,00	1,00	0,97	1,00	1,00	1,00	1,00	1,00	1,00	1,00	1,00
32	5,31	9,42	12,91	15,86	16,16	18,33	19,54	19,98	20,82	20,96	21,10	21,37	21,59	21,71	22,96	23,08	24,45	26,20
33	1,00	0,01	1,29	0,88	4,07	2,80	3,31	1,21	0,19	10,08	11,15	2,86	4,64	1,00	5,72	0,09	3,29	5,26
34	8,65	9,11	1,00	1,00	26,08	1,00	1,00	1,00	1,00	1,00	1,00	1,83	1,00	13,18	1,00	1,00	1,00	1,18
35	8,45	8,17	1,00	1,00	24,29	1,00	1,00	1,00	1,00	4,58	9,27	1,00	1,00	28,81	1,00	1,00	1,00	1,00
36	1,00	0,80	1,00	1,00	23,78	1,00	8,23	13,12	18,49	1,00	23,43	18,80	1,00	1,00	1,00	0,65	1,00	1,00
37	1,00	1,00	13,54	1,00	1,00	1,00	43,42	54,69	52,32	21,78	11,20	56,52	42,54	1,00	46,68	56,69	58,80	53,38
38	9,87	17,95	52,21	50,30	28,86	49,60	62,60	30,68	21,90	62,46	56,26	35,24	51,24	4,31	55,37	29,88	39,38	54,20

| TrkC	IGF-1 R	EphA7	ErbB4	ErbB3	Dtk	ROR1	VEGF R2	FGF R2alpha	TrkA	PDGF R beta	Tie-2	Mer	ErbB2	Axl	c-Ret	Insulin R	Tie-1	EphB6	M-CSF R	MSP R	EphB2	EphA1	EGF R
1,00	13,20	7,12	12,18	30,10	15,57	4,48	1,00	1,00	19,14	2,44	22,86	35,26	20,96	11,78	4,32	9,87	16,69	1,00	1,91	18,35	1,00	4,07	181,01
0,89	4,84	4,20	0,06	0,28	3,99	0,92	1,00	1,00	3,96	3,00	8,61	5,18	7,74	5,64	1,67	1,38	3,00	1,00	1,00	0,36	3,28	0,04	124,06
1,00	1,00	2,16	1,00	1,00	13,42	0,09	9,47	1,00	3,46	42,89	1,00	7,21	2,70	1,00	1,00	6,44	6,17	9,08	13,99	2,59	12,15	1,00	192,91
1,58	2,47	4,26	22,71	5,70	107,60	1,23	0,89	3,05	8,04	5,77	8,92	14,79	18,08	1,00	1,00	1,00	0,29	7,92	1,00	13,96	33,96	1,00	54,25
6,57	7,19	13,95	13,64	6,00	84,38	6,67	5,48	7,32	19,01	8,72	18,23	13,02	12,04	5,65	6,22	8,90	16,43	7,95	8,92	14,74	20,26	8,89	28,44
1,65	2,29	5,31	3,92	4,54	9,51	2,04	3,13	7,92	14,81	12,01	13,76	11,78	13,35	1,00	3,72	5,40	7,56	2,72	11,10	5,49	6,11	4,66	124,07
1,91	2,11	34,14	18,98	3,28	105,30	1,06	1,00	16,83	20,52	12,22	54,76	46,02	18,76	1,00	1,00	7,96	3,64	1,00	1,00	23,47	14,02	3,47	90,40
11,49	30,41	42,25	62,62	8,86	163,26	18,00	7,24	12,67	34,17	15,82	88,48	36,71	34,10	64,87	22,50	25,21	11,26	10,49	17,63	177,75	10,72	36,12	73,30
2,63	1,81	5,16	3,41	1,00	52,37	4,24	0,06	3,94	5,67	2,73	10,34	4,96	3,07	2,52	1,98	3,23	3,96	3,27	1,00	9,71	9,16	3,30	12,74
93,15	47,58	127,99	147,26	93,49	135,16	23,73	114,82	129,22	123,30	143,44	79,97	79,82	120,99	1,00	20,88	46,65	1,00	135,00	81,88	144,85	141,88	41,32	107,78
1,00	1,00	1,00	1,00	1,00	16,91	1,00	1,00	1,00	1,00	1,00	1,00	1,00	1,00	1,00	1,00	1,00	19,40	1,00	1,00	1,00	1,00	1,00	137,99
7,72	1,00	27,68	11,72	13,40	1,00	1,00	1,00	1,00	35,27	1,00	31,26	27,79	10,27	1,00	1,00	1,00	1,00	1,00	25,95	21,81	1,00	1,00	193,52
4,50	2,23	9,02	7,22	5,62	7,85	3,62	2,81	7,82	12,44	9,07	21,30	17,94	13,40	0,75	3,00	5,92	4,34	3,00	5,88	8,62	12,28	3,62	167,80
16,35	21,78	20,29	23,20	20,93	31,78	30,23	7,87	22,31	23,71	34,49	25,89	35,67	28,34	36,38	16,58	37,60	27,99	14,13	71,62	41,27	42,34	22,35	188,90
1,00	1,00	1,00	1,00	1,00	6,57	1,12	1,00	1,00	1,00	0,59	1,00	1,00	3,83	1,00	0,30	1,00	1,00	1,00	1,00	1,00	1,00	0,74	13,05
4,64	1,00	8,68	9,99	1,50	84,78	1,00	2,27	3,58	8,73	5,11	10,69	9,15	3,66	0,75	1,00	1,00	7,13	2,24	10,87	33,60	1,00	1,00	21,05
1,00	1,00	1,00	1,00	1,00	2,81	1,00	1,00	1,00	1,00	1,00	1,00	1,00	1,00	1,00	1,00	1,00	1,00	1,00	1,00	1,00	1,00	1,00	132,19
1,00	64,17	24,79	171,00	32,23	1,00	1,00	1,00	1,10	39,02	1,00	43,82	150,32	167,00	2,60	1,00	36,10	1,00	1,00	1,00	27,53	1,00	1,00	204,31
1,00	20,46	1,00	1,00	1,00	1,00	1,00	1,00	1,00	1,00	1,00	1,00	1,00	1,12	1,00	1,00	1,00	1,00	1,00	1,00	1,00	1,00	1,00	70,64
1,00	1,00	1,00	1,00	1,00	1,00	1,00	1,00	1,00	1,00	1,00	1,00	1,00	1,12	1,00	1,00	1,00	1,00	1,00	1,00	1,00	1,00	1,00	143,93
25,09	1,00	1,00	1,00	1,00	40,83	18,28	1,00	1,00	1,00	26,64	1,00	1,00	7,68	2,59	80,26	5,32	1,00	20,72	1,00	14,53	1,00	1,00	173,96
1,00	99,49	1,00	13,51	1,00	1,00	4,73	17,11	43,30	13,17	133,21	1,00	1,00	64,99	17,81	41,15	74,72	18,28	23,67	15,95	3,55	5,79	80,66	151,61
1,00	22,63	1,00	1,00	1,00	73,43	31,26	1,00	1,00	1,00	1,00	1,00	1,00	1,00	1,00	26,78	24,24	4,08	11,09	20,77	1,00	18,56	34,51	1,00
17,00	4,77	34,46	37,06	8,55	84,23	3,97	9,45	24,32	33,69	22,91	42,49	30,39	21,23	12,80	7,92	12,05	27,01	5,63	12,64	56,78	23,60	11,20	22,45
6,45	5,89	1,00	7,80	3,32	1,00	10,26	9,27	13,94	1,00	17,95	5,95	29,32	8,39	2,99	13,48	28,56	0,31	12,60	17,80	8,17	23,46	12,75	164,23
1,00	1,00	1,00	4,03	1,00	2,08	1,00	1,00	1,77	1,00	1,00	1,00	12,96	1,00	1,00	1,00	1,00	1,00	1,00	8,65	0,14	1,00	1,00	115,89
26,27	26,44	28,17	28,19	28,98	29,34	29,97	30,34	32,71	36,51	38,04	40,28	40,66	41,06	42,25	44,68	44,84	50,77	54,05	54,19	56,48	67,49	71,88	135,36
0,08	7,75	1,37	7,00	1,00	42,97	10,81	1,82	5,88	0,80	28,05	16,62	8,86	5,60	7,21	3,32	18,02	6,79	9,84	6,10	12,70	35,87	9,90	207,17
1,00	27,78	1,00	1,00	1,00	35,62	20,27	1,00	1,00	1,00	28,50	1,00	1,02	11,68	71,56	3,85	17,93	27,38	1,00	1,00	12,83	12,10	1,00	184,04
1,00	58,03	1,00	1,00	1,00	17,77	17,51	1,00	1,00	1,00	8,37	1,00	1,00	1,00	20,92	3,87	12,17	17,61	1,00	89,08	1,00	1,00	4,01	74,96
1,00	49,99	8,05	1,00	1,00	1,00	25,39	0,51	1,00	24,69	34,65	21,34	27,28	1,00	16,36	1,00	29,32	1,00	1,00	8,65	0,14	1,00	1,00	115,89
52,13	1,00	68,31	59,39	48,19	1,00	1,00	50,97	38,98	68,40	60,56	49,85	51,54	72,71	1,00	1,00	1,00	1,00	149,74	1,00	65,52	174,74	1,00	155,18
34,76	43,68	37,79	42,33	28,52	22,26	41,43	61,88	56,91	32,19	75,43	30,09	29,74	29,70	28,76	30,90	52,37	13,71	58,28	64,10	43,10	44,60	32,09	116,65

Supplemental Table 2: Normalized phospho signal values of MAPK arrays. Mean signals of double spots were normalized to positive controls after background correction. Negative and 0 values were set to 1. Patient Nr. Correspond to Patient sample list (see Tab13)

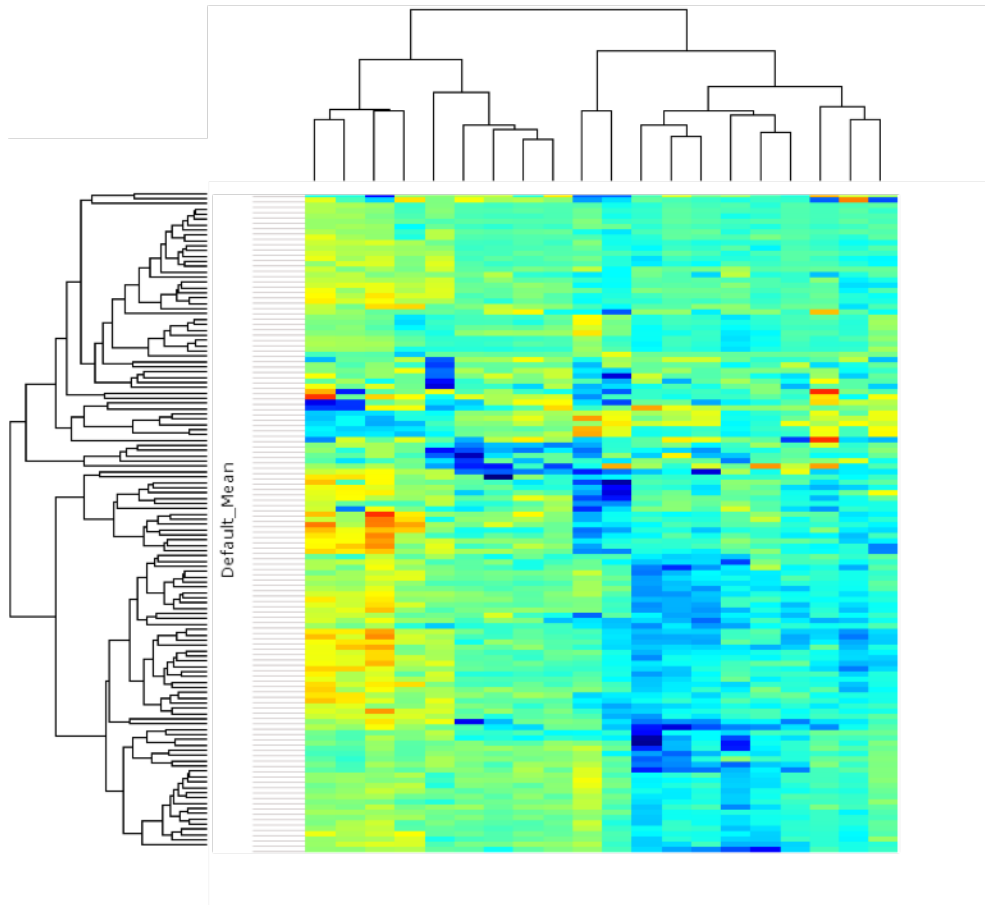| Patient Nr.	RSK2	AKT2	GSK-3 beta	p38 gamma	p70 S6 Kinase	JNK pan	Akt pan	AKT1	GSK-3 alpha/beta	p38 beta	Akt3	p38 delta	JNK3	JNK1	ERK2	ERK1	p38 alpha	MSK2	JNK2	RSK1	HSP27
1	59,58	42,70	52,49	93,40	95,33	57,23	104,02	101,92	70,56	93,29	69,98	116,91	89,33	62,47	96,67	34,15	93,58	90,49	86,55	78,13	88,44
2	3,60	131,62	5,03	135,05	4,07	70,19	115,96	57,75	66,98	2,06	9,68	119,34	2,27	4,86	88,80	138,68	169,46	71,32	61,83	3,69	149,93
3	0,64	1,42	1,00	1,08	1,24	2,06	1,90	0,56	-0,43	82,26	0,44	203,08	4,38	2,66	30,05	66,99	132,72	9,54	6,74	-0,67	112,61
5	4,32	2,36	0,39	12,18	0,45	0,53	2,70	1,53	1,30	6,43	3,98	153,28	2,38	2,92	7,92	9,24	64,06	4,37	5,72	2,16	19,82
11	4,53	11,28	2,20	4,22	6,76	4,99	5,38	19,52	8,44	16,20	41,56	4,54	11,66	17,15	7,98	3,97	41,98	10,36	18,59	76,73	10,05
6	26,44	26,82	31,58	26,70	34,66	39,59	28,51	63,73	53,84	82,48	105,19	33,62	134,67	137,46	145,91	46,14	128,28	111,79	159,80	177,26	190,81
8	21,80	25,40	48,00	40,25	59,62	65,73	63,83	96,82	51,09	216,68	192,40	45,60	193,87	196,33	200,80	192,39	210,43	211,29	242,74	244,04	234,75
9	25,05	27,74	52,04	44,25	65,53	71,54	71,45	107,15	55,23	228,35	204,10	49,18	211,86	211,27	212,43	209,88	225,30	227,96	245,28	244,41	237,00
10	26,51	36,69	172,77	20,95	131,98	44,17	65,17	87,33	192,68	80,57	106,96	38,29	83,15	86,58	97,98	25,64	92,06	127,00	114,00	164,65	225,49
13	42,80	33,03	72,05	45,93	67,09	42,10	36,99	117,16	175,59	67,22	90,79	55,47	109,53	117,84	105,45	148,68	91,63	105,77	164,59	181,40	233,06
4	10,70	17,96	10,08	9,43	17,01	19,41	15,45	21,42	31,19	38,17	66,64	49,67	51,42	52,21	67,65	114,95	46,59	61,31	123,11	141,43	207,03
7	48,18	10,35	27,86	27,18	22,85	61,77	13,86	25,63	102,71	31,66	45,54	69,21	31,25	53,94	37,39	184,22	24,72	91,86	42,59	52,34	196,67
12	42,37	26,69	25,99	35,38	31,01	46,94	37,27	94,12	94,20	20,05	39,54	57,18	60,48	45,69	33,95	46,72	26,45	137,36	72,12	39,64	99,06
15	9,24	1,00	4,16	16,46	1,00	28,59	1,00	6,43	20,16	4,87	0,25	19,24	39,73	39,70	33,80	47,78	11,48	117,07	37,17	14,25	134,54
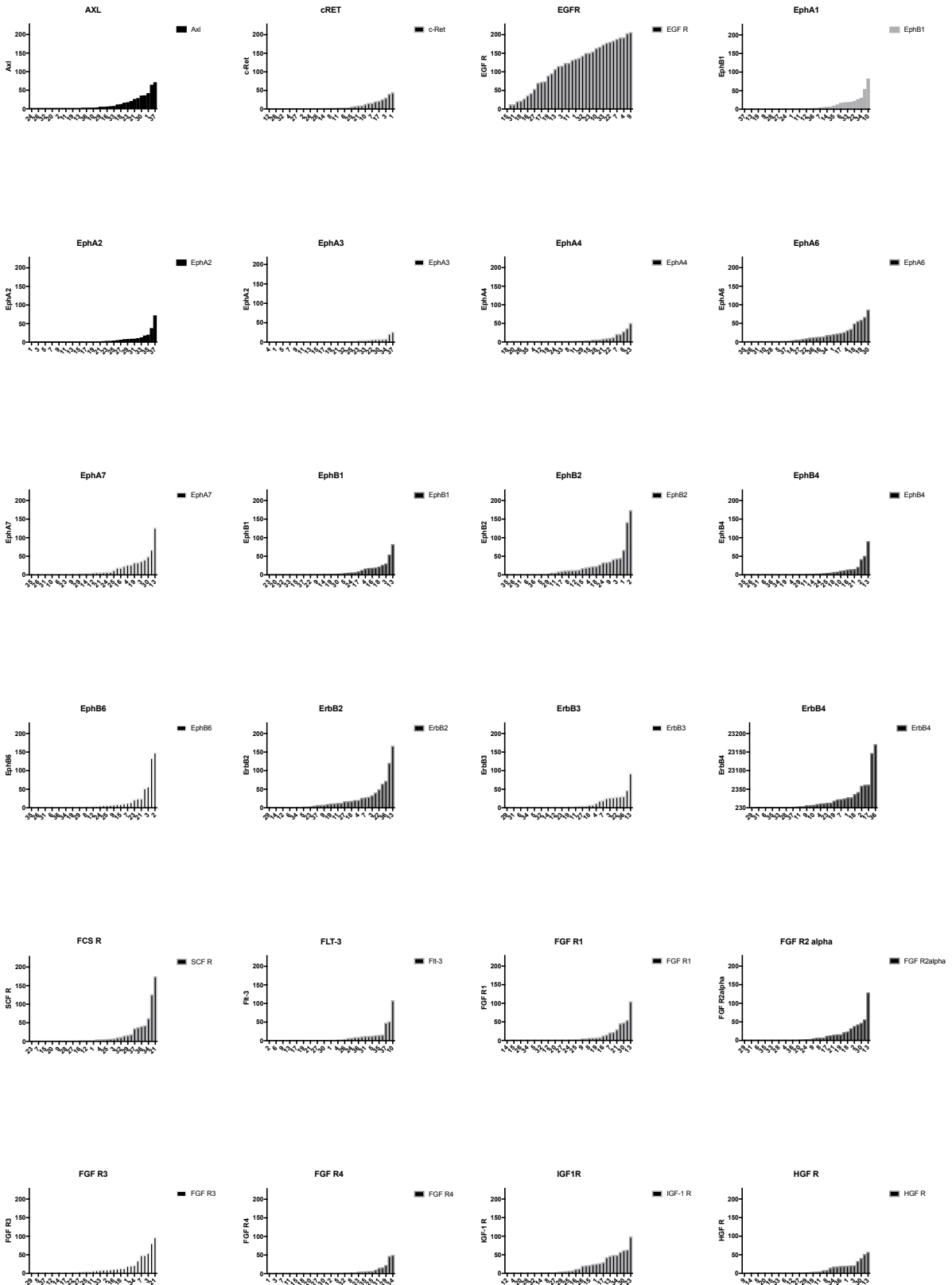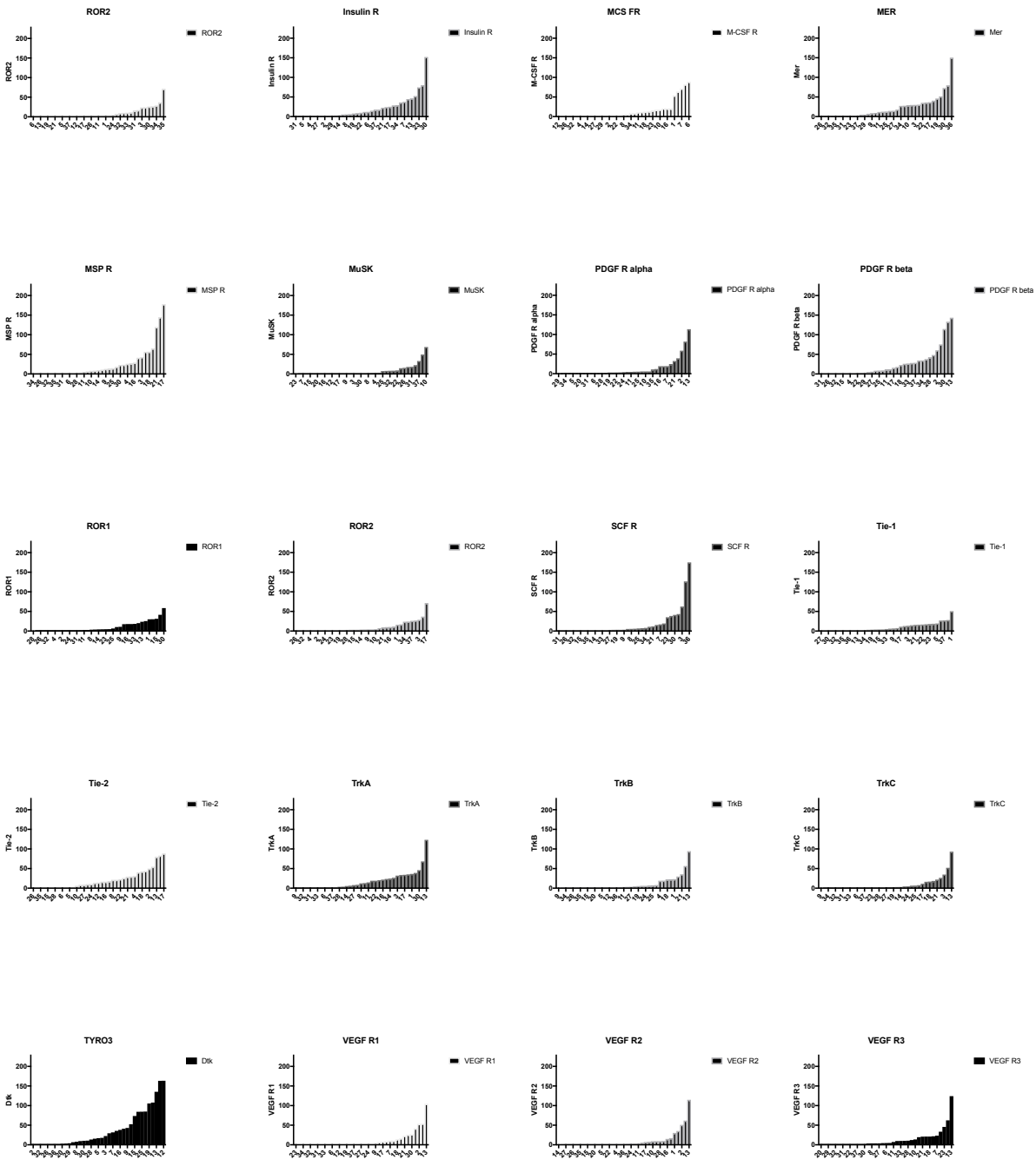
Supplemental Figure 1: Distribution of single phospho signals sorted by intensity of 33 malignant TH and TC shows a very heterogenous distribution of RTK activity

A

B

PTX QC::KineticPTK_presence

PTX QC::KineticPTK_presence

C

ratio::LFC_Mean
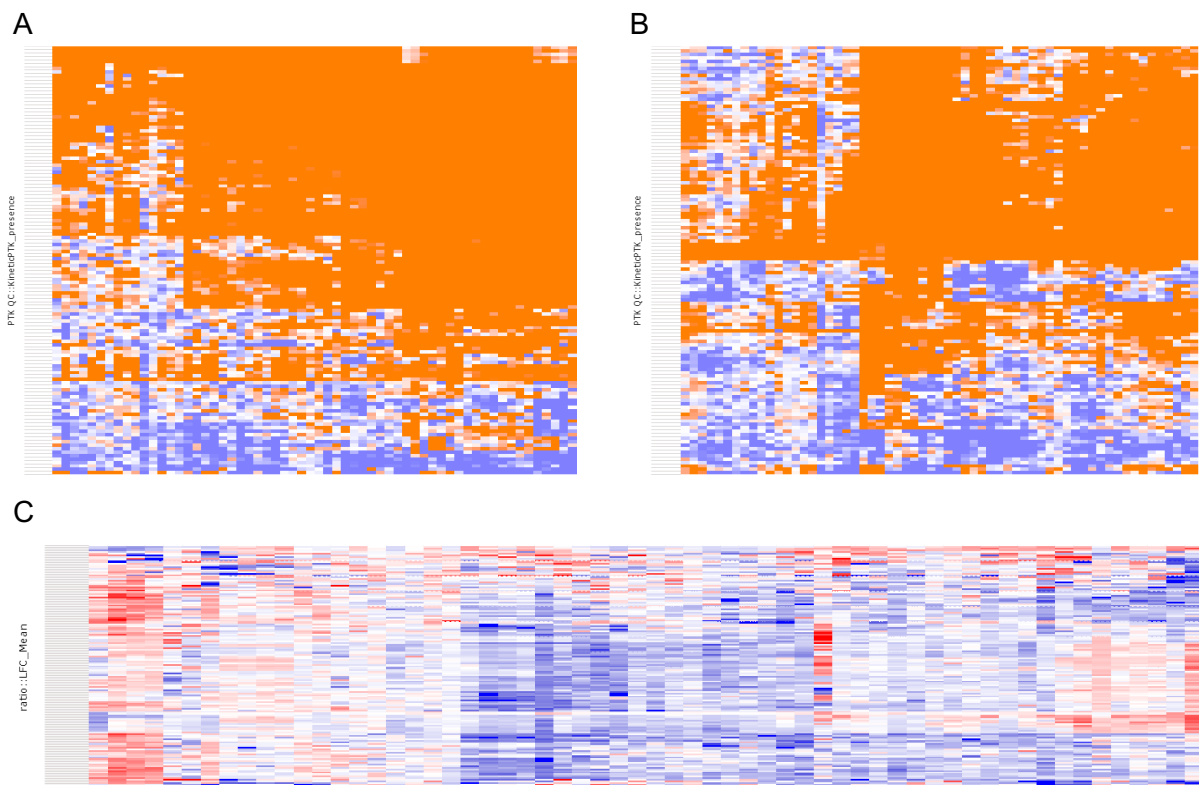
Supplemental Figure 2: Separate DMSO control (A) and sunitinib-treated (B) clusters were visualized (Supplemental Figures 2A and B, respectively). Visualization of unsupervised clustering of the ratio values (C).
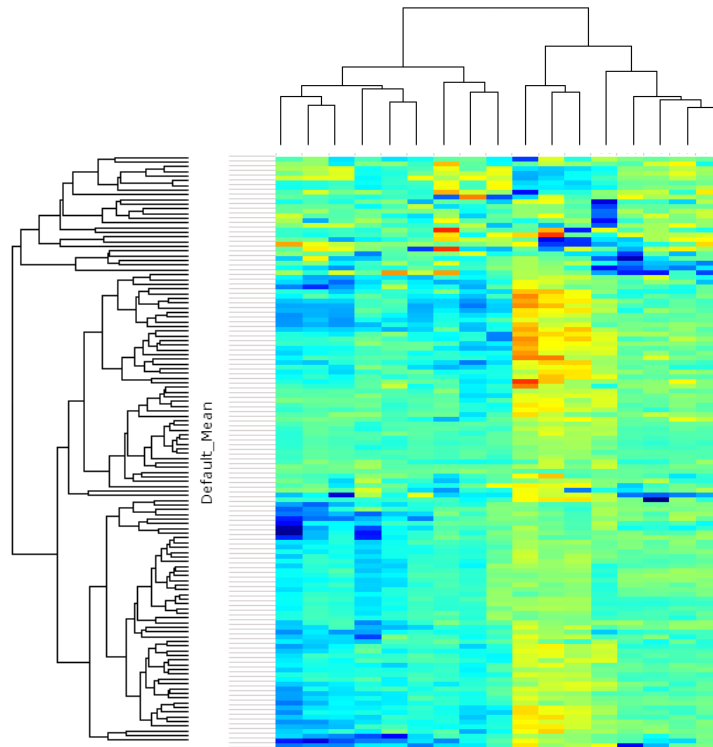
Supplemental Figure 3: Unsupervised hierarchical clustering of ratio values of resistance-induced and native cell lines for SRI generation and validation.

A

B

Supplemental Figure 4: Upstream prediction of resistance-induced and native cell lines separated by the SRI. Final score of putatively affected kinases (y-axis). The specificity score is indicated by color. The length of the bars indicate the normalized specificity score (NSS) for these kinases (NSS < 0 indicates less inhibition, NSS > 0 more inhibition in sunitinib-treated cells for the quantifier) (A). The corresponding volcano plot. Fond of the kinase indicates peptides included in the set (B).

Supplemental Figure 5: Unsupervised hierarchical clustering of ratio values of tissues for SRI generation and validation.
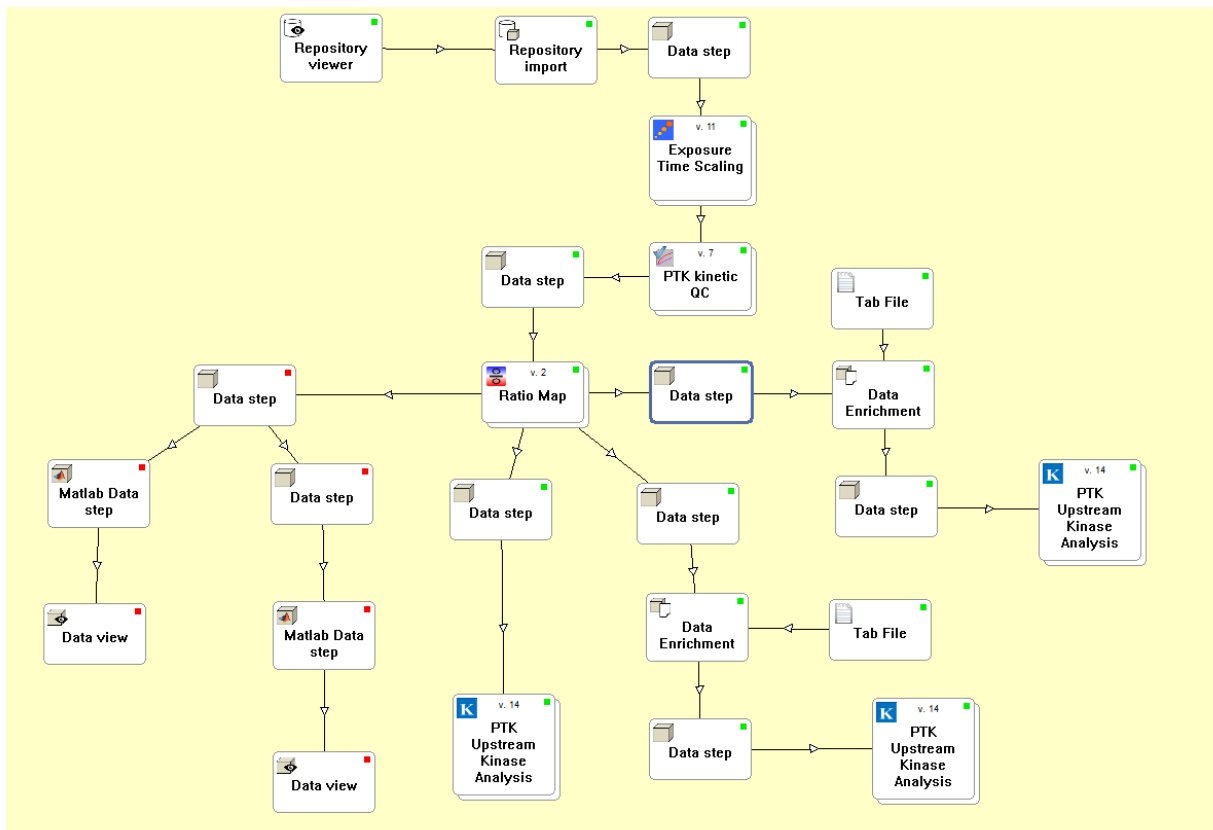
Supplemental Figure 6: Representative picture of the protocol used for PamChip analysis in the BioNavigatoR (version 6.2; PamGene, 's-Hertogenbosch, The Netherlands)

7 CURRICULUM VITAE

PERSONALIEN

Name und Vorname:	Küffer Stefan Thomas
Geburtsdatum:	25. Juni 1974
Geburtsort:	Thun (Schweiz)
Familienstand:	verheiratet
Vater:	Küffer Kurt
Mutter:	Küffer Marianne

SCHULISCHER WERDEGANG

08/1990 – 06/1996	Kollegium Karl Borromäus Altdorf, CH
05/1996	Matura Typeus C

UNIVERSITÄRER WERDEGANG

10/1996 – 03/2001	Study of Molecular Biology, Universtiy of Fribourg, CH
03/2001	Master degree in Molecular and Cell Biology (Dipl. Biol)
06/2001 – 07/2003	**Institute of Infectious Diseases (IFIK) at the Inselspital Bern and at the University of Connecticut (UConn)** Research focus: Signature tagged mutagenesis (STM) to screen mutated Aeromonas verbana in the digestive tract of Hirudo medicinalis the medical leech.

01/2004 – 09/2008	**German Cancer Research Institut (DKFZ)** in Heidelberg Research focus: Microarray analysis of prostatic intraepithelial neoplasia in frozen and formalin-fixed tissue for the detection of early prostate cancer markers; MicroRNA in precancerous and cancerous lesions of human prostate
10/2008 – 09/2012	**Institut of Pathology, University Medical Center Mannheim (UMM)** Research focus: IGF2 regulation in prostate cancer
10/2012 – Today	**Institut of Pathology, University Medical Center Göttingen (UMG), Labmanager** Research focus: Therapy resistance and response prediction to the second-line therapeutic agent sunitinib in malignant thymoma and thymic carcinoma

Publications:

1: Stefan Porubsky, Birgit Rudolph, Jens-Carsten Rückert, **Stefan Küffer**, Philipp Ströbel, Anja C. Roden, Deepali Jain, Thomas Tousseyn, Hans van Veer, Alberto Antonicelli, Tseng-tong Kuo, Juan Rosai and Alexander Marx, Primary hyalinizing clear cell carcinoma of thymus shows *EWSR1-ATF1* translocation, Histopathology, May , 2019 (accepted, in press)

2: Helen Dinter, Hanibal Bohnenberger, Julia Beck, Kirsten Bornemann-Kolatzki, Ekkehard Schütz, **Stefan Küffer,** Lukas Klein, Teri J. Franks, Anja Roden, Alexander Emmert, Marc Hinterthaner, Mirella Marino, Luka Brcic, Helmut Popper, Cleo-Aron Weis, Giuseppe Pelosi, Alexander Marx, and Philipp Ströbel, molecular classification of neuroendocrine tumors of the thymus, Journal of Thoracic Oncology (JTO), 2019 (accepted, in press)

3: Bohnenberger H, Kaderali L, Ströbel P, Yepes D, Plessmann U, Dharia NV, Yao S, Heydt C, Merkelbach-Bruse S, Emmert A, Hoffmann J, Bodemeyer J, Reuter-Jessen K, Lois AM, Dröge LH, Baumeister P, Walz C, Biggemann L, Walter R, Häupl B, Comoglio F, Pan KT, Scheich S, Lenz C, **Küffer S**, Bremmer F, Kitz J, Sitte M, Beißbarth T, Hinterthaner M, Sebastian M, Lotz J, Schildhaus HU, Wolff H, Danner BC, Brandts C, Büttner R, Canis M, Stegmaier K, Serve H, Urlaub H, Oellerich T.

Comparative proteomics reveals a diagnostic signature for pulmonary head-and-neck cancer metastasis. EMBO Mol Med. 2018 Sep;10(9).

4: **Küffer S**, Gutting T, Belharazem D, Sauer C, Michel MS, Marx A, Trojan L, Ströbel P. Insulin-like growth factor 2 expression in prostate cancer is regulated by promoter-specific methylation. Mol Oncol. 2018 Feb;12(2):256-266.

5: Venkataramani V, **Küffer S**, Cheung KCP, Jiang X, Trümper L, Wulf GG, Ströbel P. CD31 Expression Determines Redox Status and Chemoresistance in Human Angiosarcomas. Clin Cancer Res. 2018 Jan 15;24(2):460-473.

6: Grafen M, Hofmann TR, Scheel AH, Beck J, Emmert A, **Küffer S**, Danner BC, Schütz E, Büttner R, Ostendorf A, Ströbel P, Bohnenberger H. Optimized expression-based microdissection of formalin-fixed lung cancer tissue. Lab Invest. 2017 Jul;97(7):863-872

7: Bürger T, Schaefer IM, **Küffer S**, Bohnenberger H, Reuter-Jessen K, Chan JK, Emmert A, Hinterthaner M, Marx A, Ströbel P. Metastatic type A thymoma: morphological and genetic correlation. Histopathology. 2017 Apr;70(5):704-710.

8: Hu B, Simon-Keller K, **Küffer S**, Ströbel P, Braun T, Marx A, Porubsky S. Myf5 and Myogenin in the development of thymic myoid cells - Implications for a murine in vivo model of myasthenia gravis. Exp Neurol. 2016 Mar;277:76-85.

9: Bremmer F, Schallenberg S, Jarry H, **Küffer S**, Kaulfuss S, Burfeind P, Strauß A, Thelen P, Radzun HJ, Ströbel P, Honecker F, Behnes CL. Role of N-cadherin in proliferation, migration, and invasion of germ cell tumours. Oncotarget. 2015 Oct 20;6(32):33426-37.

10: Wangsa D, Chowdhury SA, Ryott M, Gertz EM, Elmberger G, Auer G, Åvall Lundqvist E, **Küffer S**, Ströbel P, Schäffer AA, Schwartz R, Munck-Wikland E, Ried T, Heselmeyer-Haddad K. Phylogenetic analysis of multiple FISH markers in oral tongue squamous cell carcinoma suggests that a diverse distribution of copy number changes is associated with poor prognosis. Int J Cancer. 2016 Jan 1;138(1):98-109.

11: Tehrany N, Kitz J, Rave-Fränk M, Lorenzen S, Li L, **Küffer S**, Hess CF, Burfeind P, Reichardt HM, Canis M, Beissbarth T, Wolff HA. High-grade acute organ toxicity and p16(INK4A) expression as positive prognostic factors in primary radio(chemo)therapy for patients with head and neck squamous cell carcinoma. Strahlenther Onkol. 2015 Jul;191(7):566-72

12: Schaefer IM, Ströbel P, Thiha A, Sohns JM, Mühlfeld C, **Küffer S**, Felmerer G, Stepniewski A, Pauli S, Agaimy A. Soft tissue perineurioma and other unusual tumors in a patient with neurofibromatosis type 1. Int J Clin Exp Pathol. 2013 Nov 15;6(12):3003-8

13: Behnes CL, Bedke J, Schneider S, **Küffer S**, Strauss A, Bremmer F, Ströbel P, Radzun HJ. Myoglobin expression in renal cell carcinoma is regulated by hypoxia. Exp Mol Pathol. 2013 Dec;95(3):307-12.

14: Belharazem D, Kirchner M, Geissler F, Bugert P, Spahn M, Kneitz B, Riedmiller H, Sauer C, **Küffer S**, Trojan L, Bolenz C, Michel MS, Marx A, Ströbel P. Relaxed imprinting of IGF2 in peripheral blood cells of patients with a history of prostate cancer. Endocr Connect. 2012 Oct 24;1(2):87-94.

15: Käcker C, Marx A, Mössinger K, Svehla F, Schneider U, Hogendoorn PC, Nielsen OS, **Küffer S**, Sauer C, Fisher C, Hallermann C, Hartmann JT, Blay JY, G, Hohenberger P, Ströbel P. High frequency of MYC gene amplification is a common feature of radiation-induced sarcomas. Further results from EORTC STBSG TL 01/01. Genes Chromosomes Cancer. 2013 Jan;52(1):93-8.

16: Feuerborn A, **Küffer S**, Gröne HJ. Forkhead factors regulate epithelial plasticity: impact on cancer progression. Cell Cycle. 2011 Aug 1;10(15):2454-60.

17: Feuerborn A, Srivastava PK, **Küffer S**, Grandy WA, Sijmonsma TP, Gretz N, Brors B, Gröne HJ. The Forkhead factor FoxQ1 influences epithelial differentiation. J Cell Physiol. 2011 Mar;226(3):710-9.

18: Manner J, Radlwimmer B, Hohenberger P, Mössinger K, **Küffer S**, Sauer C, Belharazem D, Zettl A, Coindre JM, Hallermann C, Hartmann JT, Katenkamp D, Katenkamp K, Schöffski P, Sciot R, Wozniak A, Lichter P, Marx A, Ströbel P. MYC high level gene amplification is a distinctive feature of angiosarcomas after irradiation or chronic lymphedema. Am J Pathol. 2010 Jan;176(1):34-9.

19: Srivastava PK, <u>**Küffer S**</u>, Brors B, Shahi P, Li L, Kenzelmann M, Gretz N, Gröne HJ. A cut-off based approach for gene expression analysis of formalin-fixed and paraffin-embedded tissue samples. Genomics. 2008 Jun;91(6):522-9.

20: Silver AC, Rabinowitz NM, **Küffer S**, Graf J. Identification of Aeromonas veronii genes required for colonization of the medicinal leech, Hirudo verbana. J Bacteriol. 2007 Oct;189(19):6763-72.

21: Kenzelmann M, Maertens S, Hergenhahn M, **Kueffer S**, Hotz-Wagenblatt A, Li L, Wang S, Ittrich C, Lemberger T, Arribas R, Jonnakuty S, Hollstein MC, Schmid W, Gretz N, Gröne HJ, Schütz G. Microarray analysis of newly synthesized RNA in cells and animals. Proc Natl Acad Sci U S A. 2007 Apr 10;104(15):6164-9.

22: Shahi P, Loukianiouk S, Bohne-Lang A, Kenzelmann M, <u>**Küffer S**</u>, Maertens S, Eils R, Gröne HJ, Gretz N, Brors B. Argonaute--a database for gene regulation by mammalian microRNAs. Nucleic Acids Res. 2006 Jan 1;34(Database issue):D115-8.

8   ACKNOWLEDGMENT